Silicon isotope variations in the inner solar system: Implications for planetary formation, differentiation and composition

Thomas Zambardi [a,b]*, Franck Poitrasson [a], Alexandre Corgne [c,d], Merlin Méheut [a], Ghylaine Quitté [e] and Mahesh Anand [f,g]

* Corresponding author:
Tel: 00337.86.27.29.84; e-mail: zambardi@illinois.edu

[a] *Géosciences Environnement Toulouse, CNRS – Université de Toulouse – IRD, 14 avenue Edouard Belin, 31400 Toulouse, France.*

[b] *Department of Geology – Natural History Building, University of Illinois at Urbana-Champaign, 1301 W. Green Street, 61801 Urbana, IL, USA.*

[c] *Institut de Recherche en Astrophysique et Planétologie, CNRS – Université de Toulouse, 14 avenue Edouard Belin, 31400 Toulouse, France.*

[d] *Instituto de Geociencias, Universidad Austral de Chile, Casilla 567, Valdivia, Chile*

[e] *Laboratoire de Géologie de Lyon : Terre, Planètes, Environnement, CNRS, ENS de Lyon, Université Lyon 1, 46 allée d'Italie, 69364 Lyon, France.*

[f] *Department of Physical Sciences, The Open University, Milton Keynes, MK7 6AA, UK.*

[g] *Department of Mineralogy, The Natural History Museum, London SW7 5BD, UK.*

Abstract

Accurate and precise Si isotope measurements were obtained using magnesium doping and high-resolution plasma source mass spectrometry for samples representative of the Earth, as well as lunar samples, meteorites from Mars (SNC), eucrites, a howardite, carbonaceous chondrites (CC), ordinary chondrites (OC) and enstatite chondrites (EC). Our data confirm that significant Si isotope fractionations exist among the inner solar system planetary bodies. They show that the Earth and the Moon share the same Si isotopic composition, which is heavier than all other measured bodies, in agreement with most of previous studies. At the other end of the spectrum, enstatite chondrites have the lightest Si isotope compositions. In order to precisely estimate the amount of Si that may have entered the Earth's core, we developed a refined model of Si partitioning based on continuous planetary accretion that takes into account the likely variations in T, P and fO_2 during the Earth's accretion, as well as isotopic constraints involving metal-silicate partitioning derived from both experimental and natural sample data sets.

Assuming that the difference between the isotopic signature of the bulk silicate Earth (BSE) and chondrites solely results from Si isotope fractionation during core formation, our model implies that at least ~12wt% Si has entered the Earth's core, which is greater than most of the estimates based on physical constraints on core density or geochemical mass balance calculations.

This result leads us to propose two hypotheses to explain this apparent contradiction: 1) At least part of the Earth's building blocks had a Si isotope composition heavier than that observed in chondrites (*i.e.*, $\delta^{30}Si > -0.39‰$). 2) If on the contrary the Earth accreted only from material having chondritic $\delta^{30}Si$, then an additional process besides mantle-core differentiation is required to generate a stronger isotope fractionation and lead to the observed heavy isotope composition of the bulk silicate Earth. It may be the loss of light Si isotopes

during partial planetary vaporization in the aftermath of the Moon-forming giant impact. This process, which may have affected metallic cores, required a thorough isotopic re-equilibration between core and silicate to explain the similar heavy isotope composition of the silicate portions of the Earth and the Moon.

Keywords: silicon isotopes, terrestrial planets, core formation, inner solar system

1. INTRODUCTION

The core of the Earth has been shown to have a 5-10% density deficit relative to a pure Fe-Ni alloy (Birch, 1968; Boehler, 2000; Anderson and Isaak, 2002), suggesting significant incorporation of light elements such as C, O, S and/or Si. Given the superchondritic Mg/Si ratio of the silicate Earth and assuming that terrestrial planets have a bulk composition similar to those of chondrites (*e.g.*, Jagoutz et al., 1979; Allègre et al., 1995; McDonough and Sun, 1995), Si has been considered among the most likely candidate light elements to occur in the core (*e.g.*, MacDonald and Knopoff, 1958; Allègre et al., 1995). However, the Si contribution to the light element budget of the Earth's core remains poorly constrained, reflecting the conflicting evidence from cosmochemical, experimental and theoretical studies concerning which light element(s) is/are present (*e.g.*, Poirier, 1994; Allègre et al., 1995; Sherman, 1997; Kilburn and Wood 1997; Gessmann et al., 2001; Li et al., 2001; Alfè et al., 2002; Rubie et al., 2004; Asahara et al., 2007; Badro et al., 2007; Côté et al., 2008; Corgne et al., 2009; Antonangeli et al., 2010). The determination of the Si isotope signatures (from here on expressed as permil δ^{30}Si) of chondritic and Earth materials has been proposed to provide additional constraints on the amount of Si present in the Earth's core (*e.g.*, Georg et al., 2007): for a given Si isotopic fractionation between the Earth's core and the Earth's mantle, the difference in δ^{30}Si between the silicate portion of the Earth and the bulk Earth is indeed proportional to the fraction of total Si going into the core. Assuming that the mean Earth signature can be estimated by measuring chondritic meteorites, the difference in isotopic composition between rock samples representative of the bulk silicate Earth and chondritic materials ($\Delta^{30}Si_{BSE\text{-}Bulk\ Earth} = \Delta^{30}Si_{BSE\text{-}Chond.}$) can thus be used to estimate the Si content of the core.

With the exception of Chakrabarti and Jacobsen (2010a), all recent studies indicate that chondritic Si isotope compositions are clearly distinct from the Earth's mantle signature

78 (Georg et al., 2007; Fitoussi et al., 2009; Zambardi et al., 2009; Ziegler et al., 2010; Armytage
79 et al., 2011; Fitoussi and Bourdon, 2012). All these studies consider that the $\Delta^{30}Si_{BSE\text{-}Chond.}$
80 values directly result from the Si incorporation into the Earth's core during accretion.
81 However two issues remain: (1) the measured $\Delta^{30}Si_{BSE\text{-}Chond.}$ values vary from one study to
82 another, which leads to significant variations in estimated core contents of Si and (2) the Si
83 fractionation during terrestrial accretion must be modeled more realistically in order to better
84 understand the relationship linking $\Delta^{30}Si_{BSE\text{-}Chond.}$ to the Si content of the Earth's core. To
85 further explore the usefulness of Si isotopes in this context, and in particular to be able to
86 compare the Si-core content inferred from isotope data with other independent constraints, it
87 is crucial to address these two points.

88 In addition to potential analytical bias during isotopic measurements that may be
89 adequately addressed through interlaboratory comparison of geostandard analyses (Reynolds
90 et al., 2007; Zambardi and Poitrasson, 2011), part of the uncertainty in estimating the Si
91 content of the core resides in the choice of which chondritic reference to use as a proxy for the
92 bulk Earth. This is because different chondrites types do not necessarily share the same Si
93 isotope signature, with carbonaceous and ordinary chondrites showing $\delta^{30}Si$ values notably
94 higher than enstatite chondrites (Georg et al., 2007; Fitoussi et al., 2009; Armytage et al.,
95 2011; Savage and Moynier, 2013). Furthermore, the nature of the terrestrial building blocks
96 remain hypothetical, and different Earth forming models have been proposed, requiring the
97 use of variable chondritic sources (*e.g.*, Allègre et al., 1995, 2001; Palme and O'Neill, 2003;
98 Trinquier et al., 2007; Carlson et al., 2007; Leya et al., 2008; Simon and DePaolo, 2010;
99 Javoy et al., 2010; Schönbächler et al., 2010).

100 Last but not least, another potential source of uncertainty in estimating the Si content
101 of the Earth's core comes from the use of single-stage core formation models (Georg et al.,
102 2007; Shahar et al., 2009; Ziegler et al., 2010; Armytage et al., 2011) that involve fixed

conditions of temperature (T), pressure (P) and oxygen fugacity (fO_2) throughout this protracted event. Such models neglect the continuous variations of these three parameters during core-mantle differentiation, while they are known to significantly affect Si metal-silicate partitioning (*e.g.*, Gessmann et al., 2001; Corgne et al., 2008). Furthermore, T variations are also known to affect isotope fractionation during metal-silicate melt partitioning (*e.g.*, Shahar et al., 2009, 2011; Ziegler et al., 2010). For these reasons, it is more appropriate to consider continuous core formation models (Wade and Wood, 2005; Corgne et al., 2008; Chakrabarti and Jacobsen, 2010a).

To address these issues, we have produced new Si isotope measurements for a number of terrestrial and lunar rocks, as well as Martian meteorites, eucrites, a howardite and different types of chondrites. Our analytical approach combines Mg-doping and high-resolution mass spectrometry, which improves both data accuracy and reproducibility (Zambardi and Poitrasson, 2011). A $\Delta^{30}Si_{BSE\text{-}Chond.}$ value is inferred from our data set, and incorporated into a continuous accretion elemental partitioning model (Wade and Wood, 2005; Corgne et al. 2008). Our model also considers the constraints on Si isotope metal-silicate fractionation (Ziegler et al., 2010; Shahar et al., 2009, 2011). This approach allows us to refine the estimates of Si incorporated into the Earth's core as a function of the selected chondrite type(s) that contributed matter to the growing Earth. We eventually compare the expected Si-core concentrations inferred from our model to those derived from purely physical constraints and/or geochemical mass balance calculations, and then discuss the range of possible processes and materials involved in terrestrial planet formation during the early stages of the solar system.

2. SAMPLES AND METHODS

This study focuses on the Si isotope compositions of silicate samples spanning a large

range of igneous rock compositions from the inner solar system. They include samples from the Earth (11 peridotites, 4 basalts, 1 gabbro, 1 diorite, 1 dolerite and 1 komatiite), Moon (4 basalts, and 1 norite), Mars (5 shergottites, 4 nakhlites and 1 chassignite), as well as HEDs (6 eucrites and 1 howardite), 6 ordinary chondrites, 3 carbonaceous chondrites and 2 enstatite chondrites. Each sample group consists of a variety of rocks that reflect as much as possible the geochemical diversity of their respective parent bodies. The full sample set is listed in Table 1.

For meteorites and lunar samples, the aliquots used for the analyses were taken from at least 1g of well-homogenized bulk-rock powders (or at least 0.8g for Martian meteorites) to ensure that the sample is representative of the bulk rock as far as possible even for these rare samples. For the more abundant terrestrial rock samples, powders were prepared by crushing more than 100g of starting material. Since a complete description of the analytical procedure is already given in Zambardi and Poitrasson (2011), only the main steps are summarized hereafter.

The sample solutions were prepared using an alkali fusion method adapted from Georg et al. (2006). Silicon purification was achieved by column chromatography using Biorad AG50W-X12 cationic resins. Typical Si recovery was between 95 and 100% after the decomposition and purification steps. Procedural blanks for Si were ~30ng, corresponding to less than 0.2% of the total amount of Si analyzed per sample and were thus negligible. All measurements were performed at the Observatoire Midi-Pyrénées (Toulouse, France) and at the Open University (Milton Keynes, United Kingdom) using a Neptune (Thermo) MC-ICP-MS in medium or high-resolution mode, with wet plasma conditions and slightly acidic HCl solutions (0.05M for both samples and standard). The instrumental mass bias drift was corrected simultaneously using the sample standard bracketing (SSB) technique and by adding magnesium (Mg) as an internal standard in both standard and samples. Measurements

of $^{25}Mg/^{24}Mg$ ratios were performed in the dynamic mode. The mass bias drift correction was then applied using the Russel's exponential law (Russel et al., 1978). All the data are reported in Table 1 as $\delta^{30}Si$ and $\delta^{29}Si$ (‰) relative to the NIST international standard reference material SRM 8546 (NBS-28) following the relation:

$$\delta^{xx}Si = \left(\frac{\left(^{xx}Si/^{28}Si\right)_{Sample}}{\left(^{xx}Si/^{28}Si\right)_{NBS-28}} - 1 \right) \times 1000 \quad (1)$$

where the superscript *xx* denotes the Si isotope with either mass number 30 or 29.

The long-term external reproducibility for $\delta^{30}Si$ and $\delta^{29}Si$ was given by the standard deviation of 54 measurements of BHVO-2 over three years. It yielded 0.07‰ and 0.04‰ (2SD) for $\delta^{30}Si$ and $\delta^{29}Si$, respectively. In the following, uncertainties of planetary and meteorite parent body means are computed as two standard error of the mean (2SE) rather than two standard deviation (2SD) since the purpose is to indicate how well we know the mean rather than to give a measure of the spread of a set of individual measurements around the mean (see *e.g.*, Miller and Miller, 1993). Noteworthy, these two standard error uncertainties represent a direct proxy of *t*-tests (see *e.g.,* Poitrasson et al., 2004, 2005). All literature data have been recomputed this way to be comparable. However, whether computed as 2SE or 2SD, it is important to keep in mind that these uncertainty estimates only include random errors but not systematic ones potentially associated to analytical or sampling biases.

3. RESULTS

All data are given in Table 1. Bulk rock $\delta^{30}Si$ values for inner solar system bodies range from -0.19‰ to -0.64‰. Comparison between $\delta^{30}Si$ and $\delta^{29}Si$ in a three-isotope plot shows that these Si isotope fractionations are mass dependent (Fig. 1), in agreement with previous data (*e.g.*, Douthitt, 1982; Molini-Velsko, 1986; Ding 1996; Georg et al., 2007; Fitoussi et al., 2009; Savage et al., 2010; Ziegler et al., 2010; Armytage et al., 2011).

Terrestrial mafic rocks yield $\delta^{30}Si$ ranging from -0.19‰ to -0.33‰ (Table 1; Fig 2), which includes the smaller variation range displayed by lunar mafic samples ($\delta^{30}Si$ ranging from -0.24‰ to -0.29‰) and therefore suggests the two bodies share similar isotopic features. Meteoritic samples including chondrites, rocks thought to originate from Mars and 4-Vesta all yield lighter $\delta^{30}Si$ values, ranging from -0.33‰ to -0.64‰ (Table 1; Fig. 2). Among chondrites, enstatite chondrites clearly display the lightest isotope compositions ($\delta^{30}Si_{EC}$ = -0.59‰ and -0.64‰) relative to both ordinary chondrites ($\delta^{30}Si_{OC}$ = -0.47 ± 0.01‰ (2SE, n=6)) themselves not statistically different from carbonaceous chondrites ($\delta^{30}Si_{CC}$ = -0.43 ± 0.05‰ (2SE, n=3)). As the signatures of CC and OC overlap within uncertainties, their averaged signature is reported in the following as $\delta^{30}Si_{O/CC}$ = -0.46 ± 0.02‰ (2SE, n=9). We note that Savage and Moynier (2013) found significant differences between EL and EH chondrites, with EH being enriched in light isotopes compared to EL. Although the present study does not reproduce such an extensive E-chondrite set, it should be noticed that our two EH-chondrites do not yield comparable negative values. In fact, the two EH we measured rather plot within the range of the EL chondrites analyzed by Savage and Moynier (2013). This issue thus requires additional measurements of E-chondrites to be solved.

A review of previously published data reveals significant differences between laboratories, even for the same extra-terrestrial samples and terrestrial geostandards (Georg et al., 2007; Fitoussi et al., 2009; Zambardi et al., 2009; Ziegler et al., 2010; Chakrabarti and Jacobsen, 2010a; Armytage et al., 2011, 2012; Zambardi and Poitrasson, 2011; Fitoussi and Bourdon 2012; Savage et al., 2012, Savage and Moynier, 2013, see Fig. 3). These variations may have multiple origins that remain complex to identify with certainty. Among them, sample heterogeneity is a plausible explanation, especially for rare samples like meteorites and lunar rocks given the limited amount of sample available for analyses. Armytage et al. (2011) previously noticed the effect of sample heterogeneity for the Martian meteorite

Governador Valadares, with two different preparations producing a 0.1‰ difference in $\delta^{30}Si$. In the present study, sample heterogeneity was avoided as much as possible by powdering at least 0.8g of bulk SNC or 1g of bulk chondrites, achondrites and lunar samples, prior to sample preparation. Furthermore, several methodological aspects that may influence the final results are still a subject of debate in the literature (*e.g.*, Zambardi and Poitrasson, 2011). These include for example the use of HCl or HNO_3 sample matrices (e.g. Cardinal et al., 2003; van den Boorn et al., 2009), removal of S from samples (van den Boorn et al., 2009), the use of a collision cell (Chakrabarti and Jacobsen, 2010a), operating a MC-ICP-MS under dry or wet plasma conditions and more broadly, the contrasted architectures of the plasma source mass spectrometer used. Altogether, the present data are well consistent with those of Armytage et al., (2011), especially for extra-terrestrial Si isotopic compositions (Fig. 4).

Given that the models estimating the planetary Si-core contents are highly sensitive to the $\Delta^{30}Si_{BSE\text{-}Chond.}$ value (see details in section 4.3), it is extremely important to estimate each planetary $\delta^{30}Si$ average as accurately and precisely as possible. In this study, the analytical protocol includes the use of Mg as an internal standard. This technique has been demonstrated to correct for isotope fractionation caused by rapid mass bias variations and matrix effects (Cardinal et al., 2003; Engström et al., 2006; Zambardi and Poitrasson, 2011). Combined with high-resolution mass spectrometry, it helps to significantly improve the reproducibility and accuracy of Si isotope measurements.

4. DISCUSSION

4.1. $\delta^{30}Si$ variability among planetary bodies

Planetary $\delta^{30}Si$ averages calculated from our new results as well as from recent literature data are presented in Figure 4. For terrestrial samples, the effect of magmatic differentiation has been shown to increase the amount of heavy Si isotopes in the most

227 differentiated materials (Douthitt 1982; Ding et al., 1996; Savage et al., 2011). These previous
228 results suggest that, assuming a homogeneous mantle source (see Savage et al., 2010), only
229 mafic and ultramafic materials should be considered as representative of the bulk silicate parts
230 of the solar system planetary bodies. We thus computed the isotopic composition of the bulk
231 silicate Earth (BSE) following this rule. This yields for our measurements $\delta^{30}Si_{BSE}$ = -0.27 ±
232 0.01‰ (2SE, n=19; see Table 1, Fig.4), in excellent agreement with values recently proposed
233 by Savage et al. (2010, 2011), and Fitoussi and Bourdon (2012), but heavier by ~0.1‰ than
234 that of Georg et al. (2007) and Chakrabarti and Jacobsen (2010a).
235 Four basalts and a norite sample allowed us to estimate the isotopic composition of the
236 lunar mantle (BSMo). We found $\delta^{30}Si_{BSMo}$ = -0.27 ± 0.02‰ (2SE, n=5), which is identical to
237 the Si isotope signature of the BSE (Fig. 4), and in agreement with the average computed by
238 Georg et al. (2007), Armytage et al. (2012) and Fitoussi and Bourdon (2012). However this
239 signature is significantly heavier than the signature of a lunar breccia (-0.45 ± 0.05‰, 2SE,
240 n=1) measured by Chakrabarti and Jacobsen (2010a).
241 Among the Martian meteorites studied here, the Los Angeles shergottite represents the
242 most differentiated and felspar-rich basaltic rock (Xirouchakis et al., 2002; Papike et al.,
243 2009). Like differentiated terrestrial samples, this more felsic sample was found to have a
244 heavier Si isotopic signature (Table 1). Los Angeles was thus omitted from the bulk silicate
245 Mars (BSMa) calculation with only less evolved rocks (meaning all samples but Los Angeles)
246 used to estimate the Martian mantle $\delta^{30}Si$. We thus derive a bulk silicate Mars signature
247 ($\delta^{30}Si_{BSMa}$) of -0.49 ± 0.03‰ (2SE, n=9), significantly lighter than both the $\delta^{30}Si_{BSE}$ and
248 $\delta^{30}Si_{BSMo}$ (Table 1, Fig. 4). Since Nakhlites may contain up to 1wt% of secondary minerals
249 (*e.g.*, smectite) (Bunch and Reid, 1975), their original isotopic signature could be shifted
250 toward lower $\delta^{30}Si$ values, given the generally accepted effects of low-temperature alteration
251 on Si isotopes (*e.g.*, Ziegler et al., 2005a). However, incorporation of 1% of smectite with a

252 light $\delta^{30}Si$ signature of -2‰ (*e.g.*, Ziegler et al., 2005b) would induce a maximum shift of
253 0.02‰ on bulk Nakhlites samples, which does not lead to a significantly different $\delta^{30}Si_{BSMa}$
254 value. Our $\delta^{30}Si_{BSMa}$ value is in excellent agreement with the -0.48‰ ± 0.06 (2SE, n=5)
255 estimate proposed by Armytage et al. (2011), is identical within uncertainties with the result
256 of Georg et al. (2007) and again significantly differs from the value reported by Chakrabarti
257 and Jacobsen, 2010a).

258 The study of HED meteorites helps to constrain the bulk isotope composition of their
259 parent body, most probably asteroid 4-Vesta (Consolmagno and Drake, 1977). Eucrites are
260 thought to be fragments of the asteroid's upper crust, whereas diogenites probably originated
261 from deeper levels. Howardites may be mixed breccias of eucrites and diogenites (*e.g.*,
262 Mittlefehldt, 1994). The lack of a resolvable difference in $\delta^{30}Si$ between the howardite and
263 eucrites measured in the present study suggests a homogeneous Si isotope composition for the
264 silicate portion of the HED parent body, in contrast with Li isotope compositions (Magna et
265 al., 2006). The HED signature of -0.41 ± 0.03‰ (2SE, n= 7) that we obtained is in agreement
266 with the data from Fitoussi et al. (2009), Armytage et al. (2011) and Chakrabarti and Jacobsen
267 (2010a), but differs from data by Georg et al. (2007).

268 Lastly, the chondrite averages often vary among authors (Fig. 4), notably for the O/C
269 groups. Given that the ordinary chondrites do not seem to show much isotopic differences
270 among their types (*e.g.*, H, L or LL; Table 1; Armytage et al., 2011), we tentatively attribute
271 these discrepancies to inter-laboratory biases.

272

273 **4.2. Planetary bulk Si isotopic compositions and chemical heterogeneity of the inner**
274 **solar system**

275 As previously shown in most of the recent studies, the lunar mantle and BSE have
276 similar $\delta^{30}Si$, both have significantly heavier isotope compositions than Mars, 4-Vesta and

chondrite parent bodies (*e.g.*, Georg et al., 2007; Armytage et al., 2011, 2012, Fitoussi and Bourdon 2012, see Fig. 4). Similarities between the Earth and the Moon were also observed for other isotope systems such as O (*e.g.*, Wiechert et al., 2003; Spicuzza et al., 2007; Hallis et al., 2010), Cr (*e.g.*, Lugmair and Shukolyukov, 1998), Ti (Zhang et al., 2012), Li (*e.g.*, Magna et al., 2006), W (*e.g.*, Touboul et al., 2007) and Sr (Moynier et al., 2010), thereby supporting a genetic link between the Moon and the Earth's mantle. Assuming that chondrites are the building blocks from which the terrestrial planets formed (*e.g.*, Jagoutz et al., 1979; Allègre et al., 1995; McDonough and Sun, 1995), the heavy Si isotope composition of the Earth's mantle relative to chondrites is therefore not representative of the bulk Earth. As previously discussed in the literature, incorporation of isotopically light Si into the Earth's core is a possible explanation for this "heavy mantle" (Georg et al., 2007; Shahar et al., 2009; Fitoussi et al., 2009; Ziegler et al., 2010; Chakrabarti and Jacobsen, 2010a; Armytage et al., 2011; Fitoussi and Bourdon, 2012).

The δ^{30}Si signatures of Mars and Vesta do not show such a shift with respect to chondrites. A possible explanation (further discussed in section 4.4) is that these bodies have not segregated a significant amount of Si into their core reflecting their relatively small size and different redox conditions of formation, in agreement with models of planetary differentiation (*e.g.*, Wade and Wood, 2005; Corgne et al., 2008).

To identify the process that led to the heavy Si isotope composition of the Earth's mantle, and eventually better constrain the amount of Si segregated into the Earth's core, an important objective is to obtain a precise value of the bulk-Earth signature. However current geochemical models indicate that the Earth may have accreted from C-chondrites (*e.g.*, Allègre et al., 1995, 2001; Palme and O'Neill, 2003), E-chondrites (*e.g.*, Javoy, 1995; Trinquier et al., 2007; Javoy et al., 2010), O-chondrites (*e.g.*, Carlson et al., 2007; Leya et al., 2008; Simon and de Paolo, 2010) or mixed types of chondrites (*e.g.*, Schönbächler et al.,

2010; Fitoussi and Bourdon 2012). Given that chondrites types do not all share the same Si isotope signature (Fig. 4), the bulk-Earth signature may then vary from -0.62‰ assuming a pure E-chondrites end-member, to -0.46‰ considering a pure O/C-chondrites end-member.

Given that the HED parent body and Mars did not experience significant core partitioning of Si during metal segregation (*e.g.*, Wade and Wood, 2005; Corgne et al., 2008), their mantle signature should then correspond to that of the bulk planetary body. Since the Si isotopic signature for HED samples is indistinguishable within uncertainties from that of O/C-chondrites, we infer the bulk composition of their parent body is consistent with a starting material dominated by O/C-chondrite-like materials. In contrast, our data show that the Martian isotopic composition appears slightly but significantly lighter than 4-Vesta. While this result is compatible with an O/C-chondrite-dominated Mars composition, it may betray the contribution of a significant amount of E-chondrites as well. A simple mass balance calculation can be used to give a rough estimate of the proportions of different chondrite types in the starting composition of Mars. Doing so leads to a range of 0 to 40wt% (with an average at 20wt%) E-chondrites for Mars' bulk composition. Interestingly, Sanloup et al. (1999) and Mohapatra and Murty (2003) proposed even larger contributions of E-chondrites for Mars building blocks (~70wt% E-chondrites) based on O isotope data. Despite the uncertainties of such models, these data suggest that E-chondrites could have significantly contributed to building Mars but only played a limited role in contributing to the HED parent body. Consequently, the possible distinct nature of the building blocks of 4-Vesta and Mars would argue in favor of the existence of chemical heterogeneities in the early solar system. While still a matter of debate (*e.g.*, Lewis, 1974; Morgan and Anders, 1980; Palme 2000; Taylor and Scott, 2003; Poitrasson et al., 2005), the existence of a temperature gradient in the solar nebula may have induced a chemical gradient following early condensation, with more oxidized and volatile-rich materials (C-chondrites-like) occurring preferably farther from the

Sun and more reduced materials (E-chondrites-like) occurring in the inner parts of the protoplanetary accretion disk.

4.3. Constraints on the Earth's core composition

Using the signature of the BSE estimated above ($\delta^{30}Si$ = -0.27‰) and assuming the Earth accreted from chondritic materials, the difference in isotopic composition between the bulk silicate Earth and its chondritic building blocks can be calculated using $\Delta^{30}Si_{BSE\text{-}Chond.} = \delta^{30}Si_{BSE} - \delta^{30}Si_{Chond}$. Assuming that this difference is due to metal-silicate partitioning during mantle-core differentiation, $\Delta^{30}Si_{BSE\text{-}Chond.}$ can be used to constrain both the Si concentration and isotopic composition of the core. However, the conditions under which mantle-core differentiation occurred must be known. Temperature (T) is a critical parameter for isotope fractionation and typical equilibrium fractionations scale with $1/T^2$ for high temperatures (Bigeleisen and Mayer, 1947). It is therefore generally accepted that the temperature dependence of the fractionation law can be written as:

$$\varepsilon_{Si}(T) = \delta^{30}Si_{Silicate(T)} - \delta^{30}Si_{Metal(T)} = \frac{B \cdot 10^6}{T^2} \quad (2)$$

where ε_{Si} denotes the fractionation factor of Si given in permil and defined as $\varepsilon = 1000 \times \ln(\alpha)$.

The value of the constant B has been estimated using either natural samples (7.64 ± 0.47, Ziegler et al., 2010) or from metal-silicate fractionation experiments (7.45 ± 0.41, Shahar et al., 2011). As mantle-core differentiation occurred under high-pressure conditions, pressure (P) may also have influenced Si fractionation, in particular through changes in the silicate melt structure. However, theoretical calculations performed by Shahar et al. (2009) suggest that the effect of P is only secondary. In the following, we will therefore consider that the isotope fractionation during accretion and core formation is only temperature dependent and

follows Equation (2).

Most recent work (Georg et al., 2007; Fitoussi et al., 2009; Shahar et al., 2009; Armytage et al., 2011; Fitoussi and Bourdon, 2012) has modeled Si isotope fractionation during mantle-core differentiation as a steady-state process at constant *T*, which gives the following relation:

$$\varepsilon_{Si}(T) = \frac{\Delta^{30}Si_{BSE-Chond.}}{F_{Core}} \quad (3)$$

where F_{Core} represents the Si mass fraction of the Earth present in the core. The concentration of Si in the core (C_{Si}^{Core}) is then derived from:

$$C_{Si}^{Core} = \left(\frac{m_{BSE}}{m_{Core}}\right).\left(\frac{F_{Core}}{1-F_{Core}}\right).C_{Si}^{BSE} \quad (4)$$

knowing that m_{BSE}/m_{core}, the BSE/core mass ratio, is 2.1 (see *e.g.*, Yoder, 1995) and that the concentration of Si in BSE (C_{Si}^{BSE}) is 21wt% (see *e.g.*, McDonough and Sun, 1995; O'Neill and Palme, 1998; Palme and O'Neill, 2003).

It should be noted that, in an effort to account for varying conditions of core-mantle differentiation, some authors have also considered two-stages models (Fitoussi et al. 2009), each stage corresponding to a steady-state process. The major problem with the single- or two-stage(s) approach is that geochemical and dynamical constraints indicate that core formation was a continuous process rather than a discrete one (*e.g.*, Wetherill, 1986; Canup and Asphaug, 2001; Halliday, 2008; Wood and Halliday, 2010). It is therefore more appropriate to use continuous core formation models such as the ones proposed by Wade and Wood (2005) and Corgne et al. (2008). In these models based on metal-silicate partitioning of siderophile elements, *T*, *P* and oxygen fugacity (fO_2) are allowed to continuously evolve as core formation proceeds. As these parameters have a major influence on elemental Si metal-silicate partitioning (*e.g.*, Corgne et al., 2008), it is crucial to consider their effects in details to obtain the most precise estimate of the Si content in the Earth's core. We thus use an approach

similar to that of Chakrabarti and Jacobsen (2010a), but in the present study all parameters (T, P and fO_2) are constrained by siderophile element abundances in the BSE and their metal-silicate partitioning behavior.

4.4. Model of continuous core formation

Continuous core formation is modeled as follows:

a. Core formation takes place during Earth's accretion, with final metal-silicate equilibration at the base of a homogeneous magma ocean.
b. Growth of the Earth is linearly modeled in 100 steps. At each step, added metal represents 32.3% of the added mass and is equilibrated with the total mass of the mantle. The metal then migrates to the core without further re-equilibration.
c. The pressure of final equilibration at the base of the magma ocean is assumed to increase proportionally to the pressure at the core-mantle boundary (CMB) of the growing Earth. The pressure at the base of the magma ocean is fixed at 40% of the pressure at the CMB for nickel (Ni) partitioning data (essentially pressure-dependent) to satisfy the well-constrained Ni content of the BSE (Corgne et al., 2008). This means that, at the end of accretion, the pressure at the CMB is ~135 GPa while the pressure at the base of the magma ocean is ~54 GPa.
d. The peridotite solidus as defined by Fiquet et al. (2010) provides the variation of T at the base of the magma ocean during accretion (hence during core formation (Fig. 5a)). Average T and P conditions of core formation are about 2900 K and 33 GPa, respectively.

Siderophile element abundances in the BSE have been shown to be consistent with a continuous accretion model (Wade and Wood, 2005; Corgne et al., 2008; Wood et al., 2008). In particular, nickel and vanadium provide tight constraints on the required conditions of T, P

and fO_2 during accretion and core formation, as shown in Fig. 5b. Variations of the core/BSE Si elemental ratio during accretion can be calculated with the *T*-*P*-fO_2 conditions and the parameterization of the Si metal-silicate partition coefficient (D_{Si}) given by Corgne et al. (2008):

$$\log D_{\mathrm{Si}} = 2.32(\pm 0.3) - \frac{21800}{T} - \frac{11(\pm 33)\cdot P}{T} - 2\log\left(\frac{x_{\mathrm{FeO}}^{\mathrm{Silicate}}}{x_{\mathrm{Fe}}^{\mathrm{Metal}}}\right) - \log \gamma_{\mathrm{Si}}^{\mathrm{Metal}} \quad (5)$$

where T is the temperature (K), P is the pressure (GPa), $x_{\mathrm{FeO}}^{\mathrm{Silicate}}$ is the molar fraction of FeO in the silicate mantle, $x_{\mathrm{Fe}}^{\mathrm{Metal}}$ is the molar fraction of Fe in the metallic droplet, and $\gamma_{\mathrm{Si}}^{\mathrm{Metal}}$ is the activity coefficient in the metallic phase calculated from Dresler (1989). As shown in Figure 5b for a fO_2 path satisfying siderophile element constraints (from Wood et al., 2008), the core/BSE concentration ratio of Si is poorly modeled due to large uncertainties associated with parameterizing the partitioning (Eq. 5). It is thus impossible to derive an accurate Si content of the core using this approach (Corgne et al., 2008). Values inferred this way span a huge and partly unrealistic range from 1 to 50wt%, considering 1SD uncertainty on the regression coefficients. As shown below, isotopic constraints on BSE and chondrites derived in section 3 can greatly reduce the range of estimates for the Si content of the core.

In the following, we present the procedure used to derive the isotopic signatures of core and BSE. At step *i*, the isotope signature of the added metal (AM) subsequently going to the core ($\delta^{30}Si_{AM(i)}$) can be calculated knowing the BSE isotope signature and the metal-silicate fractionation law at the base of the magma ocean:

$$\delta^{30}\mathrm{Si}_{\mathrm{AM}(i)} = \delta^{30}\mathrm{Si}_{\mathrm{BSE}(i)} - \varepsilon_{\mathrm{Si}}(T_{(i)}) \quad (6)$$

From mass-balance considerations, the following relationship can be derived between the isotope signatures at step *i* and step *i*+1:

$$\delta^{30}\mathrm{Si}_{\mathrm{BSE}(i)}\cdot m\mathrm{Si}_{\mathrm{BSE}(i)} + \delta^{30}\mathrm{Si}_{\mathrm{Chond.}}\cdot m\mathrm{Si}_{\mathrm{Chond.}} = \delta^{30}\mathrm{Si}_{\mathrm{BSE}(i+1)}\cdot m\mathrm{Si}_{\mathrm{BSE}(i+1)} + \delta^{30}\mathrm{Si}_{\mathrm{AM}(i+1)}\cdot m\mathrm{Si}_{\mathrm{AM}(i+1)} \quad (7)$$

where $m\mathrm{Si}_{\mathrm{BSE}(i)}$, $m\mathrm{Si}_{\mathrm{AM}(i)}$ and $m\mathrm{Si}_{\mathrm{Chond.}}$ are the Si mass in BSE and added metal at step *i*, and

the added Si mass from chondrites at each step, respectively. Combining (6) and (7) yields:

$$\delta^{30}\mathrm{Si}_{\mathrm{BSE}(i+1)} = \frac{\delta^{30}\mathrm{Si}_{\mathrm{BSE}(i)} \cdot m\mathrm{Si}_{\mathrm{BSE}(i)} + \varepsilon_{\mathrm{Si}}(T_{(i+1)}) \cdot m\mathrm{Si}_{\mathrm{AM}(i+1)} + \delta^{30}\mathrm{Si}_{\mathrm{Chond.}} \cdot m\mathrm{Si}_{\mathrm{Chond.}}}{m\mathrm{Si}_{\mathrm{BSE}(i+1)} + m\mathrm{Si}_{\mathrm{AM}(i+1)}} \quad (8)$$

Since we are interested in isotope signatures with respect to the initial chondritic material, $\delta^{30}\mathrm{Si}_{\mathrm{X}}$ can be replaced by $\Delta^{30}\mathrm{Si}_{\mathrm{X\text{-}Chond.}}$ in equation (8), with $\Delta^{30}\mathrm{Si}_{\mathrm{X\text{-}Chond.}} = \delta^{30}\mathrm{Si}_{\mathrm{X}} - \delta^{30}\mathrm{Si}_{\mathrm{Chond.}}$, giving:

$$\Delta^{30}\mathrm{Si}_{\mathrm{BSE-Chond.}(i+1)} = \frac{\Delta^{30}\mathrm{Si}_{\mathrm{BSE-Chond.}(i)} \cdot m\mathrm{Si}_{\mathrm{BSE}(i)} + \varepsilon_{\mathrm{Si}}(T_{(i+1)}) \cdot m\mathrm{Si}_{\mathrm{AM}(i+1)}}{m\mathrm{Si}_{\mathrm{BSE}(i+1)} + m\mathrm{Si}_{\mathrm{AM}(i+1)}} \quad (9)$$

The value of $\Delta^{30}\mathrm{Si}_{\mathrm{BSE\text{-}Chond.}}$ at the end of core formation is calculated using Eq. (9) with the initial conditions $\Delta^{30}\mathrm{Si}_{\mathrm{BSE\text{-}Chond.}(0)} = 0$ and $m\mathrm{Si}_{\mathrm{BSE}(0)} = 0$ and the final condition $m\mathrm{Si}_{\mathrm{BSE}(100)}$ given by current BSE concentration models (21wt% Si, e.g., McDonough and Sun, 1995; O'Neill and Palme, 1998), and using Eq. (5) to derive Si mass partitioning between the added metal ($m\mathrm{Si}_{\mathrm{AM}}$) and silicate ($m\mathrm{Si}_{\mathrm{BSE}}$). The isotopic signature of the core at step i is then given by the equation:

$$\Delta^{30}\mathrm{Si}_{\mathrm{Core-Chond.}(i)} = \frac{\sum_{j=1}^{i} \Delta^{30}\mathrm{Si}_{\mathrm{AM-Chond.}(j)} \cdot m\mathrm{Si}_{\mathrm{AM}(j)}}{\sum_{j=1}^{i} m\mathrm{Si}_{\mathrm{AM}(j)}} \quad (10)$$

Figure 5c presents the theoretical variations of $\Delta^{30}\mathrm{Si}_{\mathrm{BSE\text{-}Chond.}}$ during accretion for a typical oxygen fugacity path satisfying siderophile element constraints, and with the fractionation law given by Ziegler et al. (2010) (Eq. (2) with B=7.64). Given the large uncertainties on elemental partitioning which are incorporated into the model (see for instance Fig. 5b), the predicted difference in isotopic signature between BSE and chondrites is also highly uncertain, ranging between 0.03‰ and 0.5‰ in the example considered here (Fig. 5c). To circumvent this difficulty, we calculated the variation during accretion of the $\Delta^{30}\mathrm{Si}_{\mathrm{BSE\text{-}Chond.}(i)}/F_{\mathrm{Core}(i)}$ ratio, where $F_{\mathrm{Core}(i)}$ is the Si fraction of the Earth contained in the core at step i. The following relationship links $F_{\mathrm{Core}(i)}$ to the partition coefficient D_{Si}:

$$\frac{1}{F_{\mathrm{Core}(i)}} = \frac{1}{D_{\mathrm{Si}(i)}} \frac{m_{\mathrm{BSE}}}{m_{\mathrm{Core}}} + 1 \quad (11)$$

where m_{BSE}/m_{core}, the BSE/core mass ratio, equals 2.1 (e.g. Yoder, 1995). For a single step steady-state process (a single-stage of core formation at a fixed T), $\Delta^{30}Si_{BSE\text{-}Chond.}/F_{Core}$ is simply equal to ε_{Si} (Eq. 2). Considering a continuous accretion scenario, the $\Delta^{30}Si_{BSE\text{-}Chond.(i)}/F_{Core(i)}$ ratio (Fig. 6) can be seen as the integrated fractionation factor during accretion, up to step i ($\Delta^{30}Si_{BSE\text{-}Chond.(100)}/F_{Core(100)} = \varepsilon_{Si}$) and taking into account all relevant effects (effect of T on isotope fractionation, T-P-fO_2 effects on elemental Si partitioning, effect of isotope dilution in the mass-increasing BSE). An important outcome of the model is that the value of $\Delta^{30}Si_{BSE\text{-}Chond.(100)}/F_{Core(100)}$ (= ε_{Si}) at the end of accretion varies little (0.88 ± 0.06), regardless of the fO_2 path considered (all paths span a realistic range (see insert of Fig. 6), while remaining consistent with siderophile element constraints). To evaluate the total uncertainty on ε_{Si} inferred from the model, it is important to also take into account the uncertainty on T through Earth's accretion. Given that T is constrained by the peridotite solidus (Fiquet et al., 2010), we can evaluate the impact of the T uncertainty on the final ε_{Si} (or $\Delta^{30}Si_{BSE\text{-}Chond.(100)}/F_{Core(100)}$) using the uncertainties from their experiments (±150K, see Fiquet et al., 2010). This leads to an additional -0.053/+0.047 uncertainty (approximated to ±0.05), resulting in a final estimate of $\Delta^{30}Si_{BSE\text{-}Chond.(100)}/F_{Core(100)} = 0.88 \pm 0.11$. In a steady state model at constant T (Eq. (3)), this $\Delta^{30}Si_{BSE\text{-}Chond.(100)}/F_{Core(100)}$ value would correspond to core formation at a fixed T of 2940K, close to the 3000K value proposed by Ziegler et al. (2010).

In the approach detailed above, we have used the fractionation law of Ziegler et al. (2010). More generally, it can be shown that $\Delta^{30}Si_{BSE\text{-}Chond.}/F_{Core\ final}$ is proportional to B (as in Equation (3)), yielding:

$$\Delta^{30}Si_{BSE\text{-}Chond.}/F_{Core\ final} = (0.115 \pm 0.008)*B \quad (12)$$

The integrated fractionation factor can then be used together with the isotope signatures of BSE and chondrites to estimate F_{Core}, and hence the amount of Si present in the core, using Eq. (4). Thus we derive a minimum estimated Si core content of 12^{+4}_{-2}wt% using O/C-chondrites as building material for the Earth ($\Delta^{30}Si_{BSE\text{-}O/CC} = 0.19$), and a maximal 29^{+21}_{-9} wt% Si using E-chondrites ($\Delta^{30}Si_{BSE\text{-}EC} = 0.35$). Any mix of chondrite types as starting materials will thus result in a $0.19 < \Delta^{30}Si_{BSE\text{-}Chond.} < 0.35$, and therefore produce an estimated Si-core concentration in-between 12 and 29wt% (Fig. 7). The corresponding δ^{30}Si isotope signature of the core is then approximately -1.1 ± 0.2‰ according to Eq. (10).

4.5 Application of the model to literature data

Applying our model to previously published data sets from various laboratories (Georg et al., 2007; Fitoussi et al., 2009; Chakrabarti and Jacobsen 2010a; Armytage et al., 2011, 2012; Fitoussi and Bourdon 2012, Savage and Moynier 2013) yields estimated Si-core concentrations varying between about 1 and 13wt% using O/C-chondrites, and between 11wt% and 35wt% using E-chondrites (see Table 2 for details). Since the model is very sensitive to the $\Delta^{30}Si_{BSE\text{-}Chond.}$ value, it is extremely important to find the most accurate estimates of both $\delta^{30}Si_{BSE}$ and $\delta^{30}Si_{Chond.}$. In order to improve the statistical robustness of our model, below we computed a $\Delta^{30}Si_{BSE\text{-}Chond.}$ that incorporates the previously published data. Given the significant offsets in both the Georg et al. (2007) and Chakrabarti and Jacobsen (2010a) results from all other recently published data including ours, we omit the former from the calculation. Thus using data from Fitoussi et al., (2009), Savage et al., (2010), Armytage et al., (2011), Fitoussi et Bourdon (2012), Savage and Moynier (2013) and this study, we estimate an average $\delta^{30}Si_{BSE}$ = -0.28 ± 0.01‰, (2SE, n=62), $\delta^{30}Si_{O/CC.}$ = -0.46 ± 0.01‰, (2SE, n=37), and $\delta^{30}Si_{EC.}$ = -0.64 ± 0.03‰, (2SE, n=26). This result in a $\Delta^{30}Si_{BSE\text{-}O/CC} = 0.18$, which leads to minimum estimate of 12^{+3}_{-3}wt% Si expected in the core, and a $\Delta^{30}Si_{BSE\text{-}EC}$ =

0.36, leading to a maximum estimate of 31^{+19}_{-10}wt% Si expected in the core (see Table 2, Fig. 7). It is worth noting that, although absolute values are apparently shifted, data from Georg et al. (2007) lead to similar results ($\Delta^{30}Si_{BSE\text{-}O/CC}$ = 0.20 and Si-core = 13wt%, and/or $\Delta^{30}Si_{BSE\text{-}EC}$ = 0.31 and Si-core = 24wt%, see Table 2) on average.

4.6. Did the Earth accrete from chondrites only?

Assuming that mantle-core differentiation is the sole process responsible for Si isotope fractionation during Earth's formation, our model suggests that the minimum expected Si core concentration is ~12wt%, using most of the available isotopic data (Table 2, Fig. 7). Such a value exceeds most of the estimates based on the expected density of Fe-Si alloys at core conditions (*e.g.*, Sherman, 1997; Alfè et al., 2002; Dobson et al., 2003; Badro et al. 2007; Brosh et al., 2009; Antonangeli et al., 2010; Ricolleau et al., 2011; Bouhifd et al., 2012) or geochemical mass balance calculations (Allègre et al., 1995; 2001; Javoy et al., 2010). The latter usually limit the Si core content at between 1 and 7wt% (in most cases between 2 and 5wt%), with the exception of a few models (Ricolleau et al., 2011) that predict higher Si core contents, up to 11wt%.

Consequently, if the actual Si concentration of the Earth's core does not exceed 5 to 7wt%, and if mantle-core differentiation is effectively the sole process responsible for the heavy isotopic signature of the BSE, then our model does not argue in favor of an Earth purely made of chondrites, but rather implies that the Earth has at least partly accreted from non-chondritic materials. Such a scenario is worth being considered further since it has already been suggested by several other studies on the basis of, for example, non-chondritic $^{142}Nd/^{144}Nd$ ratio (Caro et al., 2008, 2010). Hence, assuming the Earth has formed from non-chondritic materials, these latter should have had a heavier Si isotope composition than that of chondrites (*i.e.,* $\delta^{30}Si > -0.39‰$).

520

521 **4.7. Silicon isotope fractionation by vaporization during a giant interplanetary impact?**

522 Preferential loss of Si to outer space during the Earth's accretion may provide an
523 alternative explanation for both the superchondritic terrestrial Mg/Si ratio and the Si isotope
524 fractionation observed between the BSE and chondrites. A study by Knight et al. (2009)
525 shows that Si vaporization from calcium-aluminum-rich inclusions (CAIs) in meteorites
526 results in very strong Si isotope fractionation. These authors found a constant fractionation
527 factor $\alpha^{29}_{Si} = 0.98985 \pm 0.00044$ for the 1600-1900°C temperature range, with the gas phase
528 being enriched in light isotopes. Considering a ~2000K Si degassing source (*e.g.*, Poitrasson
529 et al., 2004; Pahlevan and Stevenson, 2007), data from Knight et al. (2009) suggest that even
530 small amounts of vaporized Si can significantly fractionate Si isotopes. Following a simple
531 Rayleigh distillation model, we can estimate that loss of between 0.9 and 1.6wt% of the bulk
532 Earth's Si loss through volatilization can explain the isotope fractionation we measured
533 between the BSE and chondrites, without the need of Si isotope fractionation during mantle-
534 core differentiation (Fig. 8A). If one now considers a chondritic Earth with 7wt% Si core
535 content (which can be translated into a 0.12‰ decrease of the starting $\Delta^{30}Si_{BSE\text{-}Chond}$ *via*
536 mantle-core differentiation; see Fig. 7), a loss of 0.4 to 1.1wt% bulk Earth's Si is sufficient to
537 reconcile our partitioning model with isotopic observations (Fig. 8B). Interestingly, this result
538 is almost identical to the Fe loss required through partial vaporization (between 0.5 and
539 1wt%) to explain the observed Fe isotope differences between the Earth-Moon couple and the
540 other solar system planetary bodies (Poitrasson et al., 2004).

541 The most widely accepted model for lunar formation involves a violent impact
542 between the proto-Earth and a Mars-sized body (*e.g.*, Canup and Asphaug 2001; Poitrasson et
543 al., 2004; Touboul et al., 2007). In this scenario, the ejected materials should have suffered
544 significant vaporization during and after the impact, accompanied by isotope fractionation.

Elliptical trajectories of the ejecta (Cameron, 2000; Canup and Asphaug, 2001) would have facilitated the loss of light isotopes escaping from the Earth-Moon system (Poitrasson et al., 2004). This event would have been followed by a thorough homogenization process between the material that subsequently re-accreted to form the Earth and the Moon, yielding undistinguishable Si isotope compositions for the two bodies (Nimmo and Agnor, 2006; Pahlevan and Stevenson, 2007, 2011; Touboul et al., 2007). Noteworthy, the gas pressure during CAI formation was most likely different – and lower – than in the aftermath of the impact, so that the fractionation factor provided by the CAI data is possibly too high for the conditions of Earth accretion (*e.g.*, Young et al., 2002). Unfortunately, the "true" Si isotope fractionation factor during large impacts is unknown, hence this model should be considered as an end-member scenario.

While Fe and Si show significant mass-dependent isotopic differences between the Earth–Moon system, Mars and 4-Vesta (*e.g.*, Poitrasson et al., 2004; Georg et al., 2007), this is not the case for elements such as O, K and Mg (*e.g.*, Humayun and Clayton, 1995; Wiechert et al., 2001; Bourdon et al., 2010; Teng et al., 2010). The lack of observable mass-dependent interplanetary isotope fractionation may result from the large fractionations observed within planets for O, or because of analytical issues for K (see Poitrasson et al., 2004). A possible explanation for the difference between Mg on one hand and Fe and Si on the other hand could be the fact that Si and Fe occur in significant quantities in the Earth's core (*e.g.*, Shahar et al., 2009, 2011; Corgne et al., 2009; Ricolleau et al., 2011). One could thus hypothesize that the elemental losses and isotopic fractionation in Si and Fe preferentially result from the partial vaporization of metallic core components in the aftermath of the giant impact (see Poitrasson et al., 2004). Such a scenario suggests that the ejected Si-rich core particles have lost light Si isotopes to space before re-accretion. These core particles should then have acquired a heavier isotopic signature and subsequently re-equilibrated with

570 mantle components within the turbulent accretion disk of the new Earth-Moon system (*e.g.*,
571 Pahlevan and Stevenson, 2007). This process may therefore have ultimately led to an
572 isotopically heavier mantle signature. This hypothesis is in agreement with numerical
573 simulations of interplanetary impacts that show significant ejection of metallic core particles
574 (*e.g.*, Cameron, 2000). Additionally, experiments have demonstrated that the vaporization
575 flux of elements is much more effective if they are initially present in metal rather than in
576 oxide form (Wang et al., 1994).

577 The feasibility of this process can be evaluated by mass balance calculations.
578 Assuming the Earth's core contains 7wt% Si prior to the impact, and considering the need to
579 vaporize 1.6% (worst possible case, *i.e.,* using only E-chondrites, see Fig. 8) of the bulk
580 Earth's Si preferentially from the core, this means that ~10% of the Si present in the core has
581 to be lost in the aftermath of the impact, which will eventually drive the Si-core concentration
582 to 6.2wt% after re-accretion. This concentration remains very close to the initially assumed
583 7wt% Si-core content. If correct, this evaluation thus suggests that only marginal amounts of
584 Si are lost from the core after the impact, given the current uncertainties on the Si-core
585 content. This result also suggests that the minimum amount of bulk core that needs to be
586 processed in such a case is 10%. Although no upper limit can be given, this still implies that a
587 relatively limited core proportion may have been processed through this mechanism. In
588 summary, the combination of a volatilization-driven isotopic fractionation process and
589 mantle-core differentiation can produce the observed heavier Si isotope signature of the
590 silicate Earth and Moon relative to chondrites.

591

592 ## 5. CONCLUSIONS

593 Significant differences in Si isotope composition were found among planetary bodies
594 of the inner solar system, in agreement with most previous studies. The bulk silicate Earth and

595 the bulk silicate Moon have the same Si isotope composition, both are isotopically heavier
596 than O/C-chondrites, E-chondrites, achondrites from 4-Vesta and Martian meteorites. This
597 argues in favor of a common origin for the Earth and the Moon.

598 Coupling Si isotope constraints with a realistic continuous accretion core formation
599 model allows us to estimate the amount of Si incorporated into the Earth's core. Assuming
600 that mantle-core differentiation is the sole process that fractionates Si isotopes, our model
601 suggests that the Earth's core has incorporated at least ~12wt% Si. While these results are
602 consistent with Si being a major light element in the Earth's core, this refined model requires
603 higher Si core contents than permitted by geophysical and experimental constraints.

604 We propose two explanations to reconcile the geochemical, dynamical and
605 geophysical data:

606 1) The Earth has – at least partly – accreted from non-chondritic materials, the latter
607 having on average heavier Si isotopic signature than chondrites (*i.e.,* $\delta^{30}Si > -0.39‰$). Such
608 materials would be required to reduce the isotopic difference $\Delta^{30}Si_{BSE\text{-}Bulk\ Earth}$ to 0.12‰ or
609 less, hence limiting the Si core concentration to a reasonable value (*i.e.,* < 7wt%).

610 2) If instead the Earth accreted only from chondritic materials and the Si core content
611 is <12wt% as dictated by geophysical constraints, then mantle-core differentiation cannot be
612 the sole mechanism from which planetary Si isotopes variations originate. An additional
613 process is then required, particularly if the Earth accreted significant amount of E-chondrite
614 material during its formation. We propose that volatilization-driven isotopic fractionation in
615 the aftermath of the Moon's forming giant impact could be this process. This mechanism
616 could have preferentially affected the metallic core, which explains the lack of isotopic
617 variations observed for lithophile elements, such as Mg, among planetary bodies. This
618 scenario requires a final isotopic re-equilibration on a planetary scale, leading to the heavier
619 isotopic compositions of the lunar and terrestrial mantles.

620 Finally, it is clear from our modeling that the mantle-core differentiation process alone
621 cannot explain the observed terrestrial planet Si isotope compositions. Our current level of
622 knowledge however, does not allow yet favoring one of the two hypotheses (*i.e.,* non-
623 chondritic Earth and/or impact generated Si vaporization) proposed in this study.
624

625 ## Acknowledgements

626 This study would not have been possible without the allocation by the NASA's
627 CAPTEM committee of lunar rocks samples to FP. The Natural History Museum of London
628 and Meteorite Working Group is gratefully acknowledged for the provision of Martian
629 meteorites to MA, as well as the Museum National d'Histoire Naturelle de Paris for providing
630 eucrites samples to GQ. We also thank the Museum d'Histoire Naturelle de Toulouse for
631 providing aliquots of Orgueil and St Sauveur meteorites and the Field Museum of Chicago for
632 a piece of meteorite Abee. Michel Gregoire is thanked for providing part of the terrestrial
633 peridotite samples. Carole Boucayrand, Manuel Henry, Sébastien Gardoll and Jonathan
634 Prunier are gratefully acknowledged for assistance during clean-lab work, as well as Jérôme
635 Chmeleff, Rémi Freydier and Manuela Fehr for analytical assistance on Neptune
636 spectrometers. Craig Lundstrom is warmly thanked for fruitful discussions as well as for
637 English language corrections. MA thanks RCUK for a research fellowship during which this
638 collaborative project was carried out. This work has been funded by a grant from the
639 Programme National de Planétologie (PNP) of CNRS-INSU to FP. Anonymous reviewers are
640 thanked for in depth reviews that helped improving both the clarity and the quality of this
641 manuscript. Associate Editor Mark Rehkämper is also acknowledged for his work on this
642 manuscript and helpful comments.
643

644 # References
645
646 Alfè D., Gillan M.J. and Price G.D. (2002) Composition and temperature of the Earth's core
647 constrained by combining ab initio calculations and seismic data. *Earth Planet. Sci.*
648 *Lett.* **195**, 91-98.
649 Allègre C.J., Manhès G. and Lewin E. (2001) Chemical composition of the Earth and the
650 volatility control on planetary genetics. *Earth Planet. Sci. Lett.* **185**, 49-69.
651 Allègre C.J., Poirier J.P., Humler E. and Hofmann A.W. (1995) The chemical composition of
652 the Earth. *Earth Planet. Sci. Lett.* **134**, 515-526.
653 Anderson O.L. and Isaak D.G. (2002) Another look at the core density deficit of Earth's outer
654 core. *Phys. Earth Planet. Inter.* **131**, 19-27.
655 Antonangeli D., Siebert J., Badro J., Farber D.L., Fiquet G., Morard G. and Ryerson F.J.
656 (2010). Composition of the Earth's inner core from high-pressure sound velocity
657 measurements in Fe-Ni-Si alloys. *Earth Planet. Sci. Lett.* **295**, 292-296.
658 Armytage R.M.G., Georg R.B., Savage P.S., Williams H.M. and Halliday A.M. (2011)
659 Silicon isotopes in meteorites and planetary core formation. *Geochim. Cosmochim. Acta*
660 **75**, 3662-3676.
661 Armytage R.M.G., Georg R.B., Williams H.M. and Halliday A.M. (2012). Silicon isotopes in
662 lunar rocks : implications for the Moon's formation and the early history of the Earth.
663 *Geochim. Cosmochim. Acta* **77**, 504-514.
664 Asahara Y., Frost D.J. and Rubie D.C. (2007) Partitioning of FeO between magnesiowüstite
665 and liquid iron at high pressures and temperatures: implications for the composition of
666 the Earth's outer core. *Earth Planet. Sci . Lett.* **257**, 435-449.
667 Badro J., Fiquet G., Guyot F., Gregoryanz E., Occelli F., Antonangeli D. and d'Astuto M.
668 (2007) Effect of light elements on the sound velocities in solid iron: Implications for the
669 composition of Earth's core. *Earth Planet. Sci. Lett.* **254**, 233-238.

670 Bigeleisen J. and Mayer M.G. (1947) Calculation of equilibrium constants for isotopic
671 exchange reactions. *J. Chem. Phys.* **15**, 261-267.
672 Birch F. (1968) Density and composition of mantle and core. *J. Geophys. Res.* **69**, 4377-4388.
673 Boehler R. (2000) High-pressure experiments and the phase diagram of lower mantle and core
674 materials. *Rev. Geophys.* **38**, 221-245.
675 Bourdon B., Tipper E.T., Fitoussi C. and Stracke A., (2010) Chondritic Mg isotope
676 composition of the Earth. *Geochim. Cosmochim. Acta* **74**, 5069-5083.
677 Brosh E., Makov G. and Shneck R.Z. (2009) Thermodynamic analysis of high-pressure phase
678 equilibria in Fe–Si alloys, implications for the inner-core. *Phys. Earth Planet. Inter.*
679 **172**, 289-298.
680 Bunch T.E. and Reid A.M. (1975) The Nakhlites Part 1. Petrography and mineral chemistry.
681 *Meteoritics* **10**, 303-315.
682 Cameron A.G.W. (1997) The origin of the Moon and the single impact hypothesis. *Icarus*
683 **126**, 126-137.
684 Cameron, A.G.W., 2000. Higher-resolution simulations of the giant impact. In: Canup, R.M.,
685 Righter, K. (Eds.), Origin of the Earth and Moon. The University of Arizona Press,
686 Tucson, pp. 133-144.
687 Canup R.M. and Asphaug E. (2001) Origin of the Moon in a giant impact near the end of the
688 Earth's formation. *Nature* **412**, 708-712.
689 Cardinal D., Alleman L.Y., de Jong J., Ziegler K. and Andre L. (2003) Isotopic composition
690 of silicon measured by multicollector plasma source mass spectrometry in dry plasma
691 mode. *J. Anal. Atom. Spectro.* **18**, 213–218.
692 Carlson R.W., Boyet M. and Horan M. (2007) Chondrite barium, neodymium, and samarium
693 isotopic heterogeneity and early earth differentiation. *Science* **316**, 1175-1178.
694 Chakrabarti R. and Jacobsen S.B. (2010a). Silicon isotopes in the inner Solar System:

implications for core formation, solar nebular processes and partial melting. *Geochim. Cosmochim. Acta* **74**, 6921-6933.

Chakrabarti R. and Jacobsen S.B. (2010b) The isotopic composition of magnesium in the inner Solar System. *Earth. Planet. Sci. Lett.* **293**, 349-358.

Consolmagno, G.J., Drake, M.J., 1977. Composition and evolution of the eucrite parent body: Evidence from rare earth elements. Geochimica et Cosmochimica Acta, 41: 1271-1282.

Corgne A., Keshav S., Wood B.J., McDonough W.F. and Fei Y. (2008) Metal–silicate partitioning and constraints on core composition and oxygen fugacity during Earth accretion. *Geochim. Cosmochim. Acta* **72**, 574-589.

Corgne A., Siebert J. and Badro J. (2009) Oxygen as a light element: a solution to single-stage core formation. *Earth Planet. Sci. Lett.* **288**, 108-114.

Côté A.S., Vocadlo L. and Brodholt J.P. (2008) The effect of silicon impurities on the phase diagram of iron and possible implications for the Earth's core structure. *J. Phys. Chem. Solids* **69**, 2177-2181.

Ding T., Jiang S., Wan D., Li Y., Li J., Song H., Liu Z. and Yao X. (1996) Silicon isotope geochemistry. *Geological Publishing House*, Beijing, 125 p.

Dobson D.P., Crichton W.A., Bouvier P., Vocadlo L. and Wood I.G. (2003) The equation of state of CsCl-structure FeSi to 40 GPa: implications for silicon in the Earth's core. *Geophys. Res. Lett.* **30**, 1014.

Douthitt C.B. (1982) The geochemistry of the stable isotopes of silicon. *Geochim. Cosmochim. Acta* **46**, 1449-1458.

Dresler W. (1989) Activities of silicon and carbon in the Fe-C-Si liquid system. Ironmaking *Conf. Proc.* **48**, 83-88.

Engström E., Rodushkin I., Baxter D.C. and Öhlander B. (2006) Chromatographic purification for the determination of dissolved silicon isotopic compositions in natural

720 waters by high resolution multicollector inductively coupled plasma mass spectrometry.
721 *Anal. Chem.* **78**, 250-257.
722 Fiquet G., Auzende A.L., Siebert J., Corgne A., Bureau H., Ozawa H. and Garbarino G.
723 (2010) Melting of peridotite to 140 GPa. *Science* **329**, 1516-1518.
724 Fitoussi C., Bourdon B., Kleine T., Oberli F. and Reynolds B.C. (2009) Si isotope systematics
725 of meteorites and terrestrial peridotites: implications for Mg/Si fractionation in the solar
726 nebula and for Si in the Earth's core. *Earth Planet. Sci. Lett.* **287**, 77-81.
727 Fitoussi C., Bourdon B. (2012) Silicon isotope evidence against an enstatites chondrite Earth.
728 *Sciencexpress*, 1 March 2012, 1-4.
729 Georg R.B., Halliday A.N., Schauble E.A. and Reynolds B.C. (2007) Silicon in the Earth's
730 core. Nature 447, 1102-1106.
731 Georg R.B., Reynolds B.C., Frank M. and Halliday A.N. (2006). New sample preparation
732 techniques for the precise determination of the Si isotope composition of natural
733 samples using MC-ICP-MS. *Chem. Geol.* **235**, 95-104.
734 Gessmann C.K., Wood B.J., Rubie D.C. and Kilburn M.R. (2001) Solubility of silicon in
735 liquid metal at high pressure: implications for the composition of the Earth's core. *Earth*
736 *Planet. Sci. Lett.* **184**, 367-376.
737 Hallis L.J., Anand M., Greenwood R.C., Miller M.F., Franchi I.A. and Russell S.S. (2010)
738 The oxygen isotope composition, petrology and geochemistry of mare basalts :
739 Evidence for large-scale compositional variation in the lunar mantle. *Geochim.*
740 *Cosmochim. Acta* **74**, 6885-6899.
741 Halliday A.N. (2008) A young Moon-forming giant impact at 70–110 million years
742 accompanied by late-stage mixing, core formation and degassing of the Earth.
743 *Phil.Trans. R. Soc. A.* **366**, 4163-4181.
744 Jagoutz E., Palme H., Baddenhausen K., Blum M., Cendales G., Dreibus B., Spettel V.,

745 Lorenz V. and Wanke H. (1979). The abundances of major, minor and trace elements in
746 the Earth's mantle as derived from primitive ultramafic nodules. *Proc. Lunar Planet.*
747 *Sci. Conf.* **10**, 2031-2050.
748 Javoy M. (1995) The integral enstatite chondrite model of the Earth. *Geophys. Res. Lett.* **22**,
749 2219-2222.
750 Javoy M., Kaminski E., Guyot F., Andrault D., Sanloup C., Moreira M., Labrosse S., Jambon
751 A., Agrinier P., Davaille A. and Jaupart C. (2010) The chemical composition of the
752 Earth: Enstatite chondrite models. *Earth Planet. Sci. Lett.* **293**, 259-268.
753 Kilburn M.R., Wood B.J. (1997) Metal-silicate partitioning and the incompatibility of S and
754 Si during core formation. *Earth Planet. Sci. Lett.* **152**, 139-148.
755 Knight K.B., Kita N.T., Mendybaev R.A., Richter F.M., Davis A.M. and Valley J.W. (2009)
756 Silicon isotopic fractionation of CAI-like vacuum evaporation residues. *Geochim.*
757 *Cosmochim. Acta* **73**, 6390-6401.
758 Lewis J.S. (1974) The temperature gradient in the solar nebula. *Science* **186**, 440-443.
759 Leya I., Schönbächler M., Wiechert U., Krähenbühl U. and Halliday A.N. (2008) Titanium
760 isotopes and the radial heterogeneity of the solar system. *Earth Planet. Sci. Lett.* **266**,
761 233-244.
762 Li J., Fei Y., Mao H.K., Hirose K., Shieh S.R. (2001) Sulfur in the Earth's inner core. *Earth*
763 *Planet. Sci. Lett.* **193**, 509-514.
764 Liu Y., Spicuzza M.J., Craddock P.R., Day J.M.D., Valley J.W., Dauphas N. and Taylor L.A.
765 (2010) Oxygen and iron isotope constraints on near-surface fractionation effects and the
766 composition of lunar mare basalt source regions. *Geochim. Cosmochim. Acta* **74**, 6249-
767 6262.
768 Lugmair G.W. and Shukolyukov A. (1998) Early solar system timescales according to ^{53}Mn-
769 ^{53}Cr systematics. *Geochim. Cosmochim. Acta* **62**, 2863-2886.

MacDonald G.J.F. and Knopoff L. (1958) On the chemical composition of the outer core. *Geophys. J. Astron. Soc.* **1**, 284-297.

Magna T., Wiechert U., Halliday A. N. (2006) New constraints on the lithium isotope compositions of the Moon and terrestrial planets. *Earth. Planet. Sci. Lett.* **243**, 336-353.

McDonough W.F., Sun S.-S. (1995) The composition of the Earth. *Chem. Geol.* **120**, 223-253.

Miller J.C., Miller, J.N., (1993) Statistics for analytical chemistry. Ellis Horwood, New York, 233 pp.

Mittlefehldt D.W. (1994) The genesis of diogenite and HED parent body petrogenesis. *Geochim. Cosmochim. Acta* **58**, 1537-1552.

Molini-Velsko C., Mayeda T.K., Clayton R.N., (1986) Isotopic composition of silicon in meteorites. *Geochim. Cosmochim. Acta* **50**, 2719-2726.

Mohapatra R.K. and Murty S.V.S. (2003) Precursors of Mars: constraints from nitrogen and oxygen isotopic compositions of martian meteorites. *Meteor. Planet. Sci.* **38**, 225-241.

Morgan J.W. and Anders E. (1980) Chemical composition of Earth, Venus, and Mercury. *Proc. Natl. Acad. Sci.* **77**, 6973-6977.

Moynier F., Agranier A., Hezel D.C. and Bouvier A. (2010) Sr stable isotope composition of Earth, the Moon, Mars, Vesta and meteorites. *Earth Planet. Sci. Let*. **300**, 359-366.

Nimmo F. and Agnor C.B. (2006) Isotopic outcome of N-body accretion simulations: constraints on equilibration processes during large impacts from Hf/W observations. *Earth Planet. Sci. Lett.* **243**, 26-43.

O'Neill H.S.C. and Palme H. (1998) Composition of the silicate Earth: implications for accretion and core formation. In: Jackson, I. (Ed.), The Earth's mantle: composition, structure, and evolution. Cambridge University Press, Cambridge, pp. 3-126.

Pahlevan K. and Stevenson D.J. (2007) Equilibration in the aftermath of the lunar-forming

giant impact. *Earth Planet. Sci. Lett.* **262**, 438-449.

Pahlevan K., Stevenson D.J., Eiler J.M. (2011) Chemical fractionation in the silicate vapor atmosphere of the Earth. *Earth Planet. Sci. Lett.* **301**, 433-443.

Palme H. (2000) Are there chemical gradients in the inner solar system? *Space Sci. Rev.* **92**, 237-262.

Palme H. and O'Neill H.S.C (2003) Cosmochemical estimates of mantle composition. In: Carlson R.W. (Ed.), Treatise on Geochemistry, The mantle and core, vol. 2, Elsevier Press, New York, pp. 1-38.

Papike J.J., Karner J.M., Shearer C.K. and Burger P.V. (2009) Silicate mineralogy of martian meteorites. *Geochim. Cosmochim. Acta* **73**, 7443-7485.

Poirier J.-P. (1994) Light elements in the Earth's outer core: a critical review. *Phys. Earth Planet. Inter.* **85**, 319-337.

Poitrasson, F., 2009. Probes of the ancient and the inaccessible. Science, 323: 882-883.

Poitrasson F., Halliday A.N., Lee D.C., Levasseur S. and Teutsch N. (2004) Iron isotope differences between Earth, Moon, Mars and Vesta as possible records of contrasted accretion mechanisms. *Earth Planet. Sci. Lett.* **223**, 253-266.

Poitrasson F., Levasseur S. and Teutsch N. (2005) Significance of iron isotope mineral fractionation in pallasites and iron meteorites for the core–mantle differentiation of terrestrial planets. *Earth Planet. Sci. Lett.* **234**, 151-164.

Reynolds B.C., Aggarwal J., André L., Baxter D., Beucher C., Brzezinski M.A., Engström E., Georg B., Land M., Leng M.J., Opfergelt S., Rodushkin I., Sloane H.J., Van den Boorn S.H.J.M., Vroon P.Z. and Cardinal D. (2007). An inter-laboratory comparison of Si isotope reference materials. *J. Anal. Atom. Spectrom.* **22**, 561-568.

818 Ricolleau A., Fei Y., Corgne A., Siebert J., Badro J. (2011) Oxygen and silicon contents of
819 Earth's core from high pressure metal–silicate partitioning experiments. *Earth Planet.*
820 *Sci. Lett.* **310**, 409-421.
821 Rubie D.C., Gessmann C.K. and Frost D.J. (2004) Partitioning of oxygen during core
822 formation on the Earth and Mars. *Nature* **429**, 58-61.
823 Russell W.A., Papanastassiou D.A. and Tombrello T.A. (1978) Ca isotope fractionation on
824 the Earth and other solar system materials. *Geochim. Cosmochim. Acta* **42**, 1075-1090.
825 Sanloup C., Jambon A. and Gillet P. (1999) A simple chondritic model of Mars. *Phys. Earth*
826 *Planet. Inter.* **112**, 43-54.
827 Savage P.S., Georg R.B., Armytage R.M.G, Williams H.M. and Halliday A.N. (2010) Silicon
828 isotope homogeneity in the mantle. *Earth Planet. Sci. Lett.* **295**, 139-146.
829 Savage P.S., Georg R.B., Williams H.M., Burton K.W. and Halliday A.N. (2011) Silicon
830 isotope fractionation during magmatic differenciation. *Geochim. Cosmochim. Acta* **75**,
831 6124-6139.
832 Savage P.S., Moynier F. (2013) Silicon isotopic variation in enstatites meteorites: clues to
833 their origin. *Earth Planet. Sci. Lett.*, *accepted manuscript*.
834 Schauble E.A. (2004) Applying stable isotope fractionation theory to new systems. *Review*
835 *Mineral. Geochem.* **55**, 65-111.
836 Shahar A., Ziegler K., Young E.D., Ricolleau A., Schauble E.A. and Fei Y. (2009)
837 Experimentally determined Si isotope fractionation between silicate and Fe metal and
838 implications for Earth's core formation. *Earth Planet. Sci. Lett.* **288**, 228-234.
839 Shahar A., Hillgren V.J., Young E.D., Fei Y., Macris C.A. and Deng L. (2011) High
840 temperature Si isotope fractionation between iron metal and silicate. *Geochim.*
841 *Cosmochim. Acta* **75**, 7688-7697.
842 Sherman D.M. (1997) The composition of the Earth's core: constraints on S and Si vs.

temperature. *Earth Planet. Sci. Lett.* **153**, 149-155.

Schönbächler M., Carlson R.W., Horan M.F., Mock T.D. and Hauri E.H. (2010) Heterogeneous accretion and the moderatly volatile element budget of Earth. *Science* **328**, 884-887.

Simon J.I. and DePaolo D.J. (2010) Stable calcium isotopic composition of meteorites and rocky planets. *Earth Planet. Sci. Lett.* **289**, 457–466.

Spicuzza M.J., Day J.M.D., Taylor L.A. and Valley J.W. (2007) Oxygen isotope constraints on the origin and differentiation of the Moon. *Earth Planet. Sci. Lett.* **253**, 254-265.

Taylor G.J. and Scott E.R. (2003) Mercury. In: Davis, A.M. (Ed.), Treatise on Geochemistry, Meteorites, Comets, and Planets, vol. 1., Elsevier Press, New York, pp. 477-485.

Teng F.Z., Li W.Y., Ke S., Marty B., Dauphas N., Huang S.C., Wu F.Y., Pourmand, A. (2010) Magnesium isotopic composition of the Earth and chondrites. *Geochim. Cosmochim. Acta* **74**, 4150-4166.

Touboul M., Kleine T., Bourdon B., Palme H. and Wieler R. (2007) Late formation and prolonged differentiation of the Moon inferred from W isotopes in lunar metals. *Nature* **450**, 1206-1209.

Trinquier A., Birck J.-L. and Allègre C.J. (2007) Widespread ^{54}Cr heterogeneity in the inner solar system. *Astrophys. J.* **655**, 1179-1185.

Van den Boorn S.H.J.M., Vroon P.Z., Van Bergen M.J. (2009) Sulfur-induced offset in MC-ICP-MS silicon-isotopes measurements. *J. Anal. Atom. Spect.* **24**, 1111-1114.

Wade J. and Wood B.J. (2005) Core formation and the oxidation state of the Earth. *Earth Planet. Sci. Lett.* **236**, 78-95.

Wang J., Davis A.M., Clayton R.N., Mayeda T.K. (1994) Kinetic isotopic fractionation during the evaporation of the iron oxide from the liquid state. *Lunar Planet. Sci.* **24**, 1479-1480.

868 Weyer S., Anbar A.D., Brey G.P., Munker C., Mezger K. and Woodland A.B. (2005) Iron
869 isotope fractionation during planetary differentiation. *Earth. Planet. Sci Lett.* **240**, 251-
870 264.
871 Wetherill G.W. (1986) Accumulation of the terrestrial planets and implications concerning
872 lunar origin. In "Origin of the Moon", Lunar and Planetary Institute, Houston, pp. 519-
873 550.
874 Wiechert U., Halliday A.N., Lee D.C., Snyder G.A., Taylor L.A. and Rumble D. (2003)
875 Oxygen isotopes and the Moon forming giant impact. *Science* **294**, 345-348.
876 Wood B.J. and Halliday A.N. (2010) The lead isotopic age of the Earth can be explained by
877 core formation alone. *Nature* **465**, 767-770.
878 Wood B.J., Wade J. and Kilburn M.R. (2008) Core formation and the oxidation state of the
879 Earth: Additional constraints from Nb, V and Cr partitioning. *Geochim. Cosmochim.*
880 *Acta* **72**, 1415-1426.
881 Xirouchakis D., Draper D., Schwandt C.S., Lanzirotti A. (2002) Crystallization conditions of
882 Los Angeles, a basaltic Martian meteorite. *Geochim. Cosmochim. Acta* **66**, 1867-1880.
883 Yoder C.F. (1995) Astrometric and geodetic properties of the Earth and the solar system. In:
884 Ahrens, T.J. (Ed.), Global Earth Physics: A Handbook of Physical Constants. American
885 Geophysical Union, Washington D.C., pp. 1-31.
886 Young E.D., Galy A., Nagahara H. (2002) Kinetic and equilibrium mass-dependant isotope
887 fractionation laws in nature and their geochemical and cosmochemical significance.
888 Geochim. Cosmochim. Acta 66, 1095-1104.
889 Zambardi T., Poitrasson F., Quitté G., Anand M. (2009) Silicon isotope variations in the Earth
890 and meteorites. *Geochim. Cosmochim. Acta* **73**, A1497.
891 Zambardi T. and Poitrasson F. (2011) Precise determination of silicon isotopes in silicate rock
892 reference materials by MC-ICP-MS. *Geostand. Geoanal. Res.* **34**, 89-99.

893 Zhang J., Dauphas N., Davis A., Leya I., Fedkin A. (2012) The proto-Earth as a significant
894 source of lunar material. *Nature Geoscience* **5**, 251-255.
895 Ziegler K., Chadwick O.A., Brzezinski M.A. and Kelly E.F. (2005a) Natural variations of
896 δ^{30}Si ratios during progressive basalt weathering, Hawaiian Islands. *Geochim.*
897 *Cosmochim. Acta* **69**, 4597-4610.
898 Ziegler K., White A.F. and Brzezinski M.A. (2005b) δ^{30}Si systematics in a granitic saprolite,
899 Puerto Rico. *Geol. Soc. Amer.* **33**, 817-820.
900 Ziegler K., Young E.D., Schauble E.A. and Wasson J.T. (2010) Metal–silicate silicon isotope
901 fractionation in enstatite meteorites and constraints on Earth's core formation. *Earth*
902 *Planet. Sci. Lett.* **295**, 487-496.
903

Figure Captions:

Fig. 1: Three-isotope plot showing $\delta^{29}Si$ vs. $\delta^{30}Si$ for individual analyses of all the samples from this study. The dashed line represents the theoretical mass dependent fractionation slope defined as: $\delta^{29}Si = \delta^{30}Si \times 0.5092$. The long-term reproducibility (2SD) is shown in the bottom left quadrant of the figure.

Fig. 2: $\delta^{30}Si$ values relative to NBS-28 for terrestrial and extraterrestrial samples. Uncertainties for individual samples are given as 2SE, computed as $2SD/\sqrt{(n-1)} \times t$, where t is the Student's correcting factor (Platzner et al., 1997). BSMa stands for bulk silicate Mars, and BSMo means bulk silicate Moon. All data are from Table 1.

Fig. 3: Comparison of published $\delta^{30}Si$ data relative to NBS-28 for samples from planetary bodies in the inner solar system. Uncertainties are given as 2SE, computed as $2SD/\sqrt{(n-1)} \times t$, where t is the Student's correcting factor (Platzner et al., 1997). AGV-2 data is from Zambardi and Poitrasson, (2011). C.C. = carbonaceous chondrites, E.C. = enstatites chondrites, R.M. = reference materials.

Fig. 4: Comparison of $\delta^{30}Si$ averages relative to NBS-28 for planetary bodies in the inner solar system from this and previous work. All uncertainties are given as ± 2SE.

Fig. 5: Model of continuous core formation during Earth's accretion (Wade and Wood, 2005; Corgne et al., 2008; Wood et al., 2008). (a) Variations of T of last equilibration (at the base of the magma ocean) and FeO content of the BSE during accretion. The T profile is defined by the peridotite solidus (Fiquet et al., 2010). FeO variations correspond to the three-step profile proposed by Wood et al. (2008). Such temperatures and FeO variations lead to modeled depletions of moderately siderophile elements in the BSE consistent with observations (as shown for Ni and V in (b)). (b) Modeled core/BSE variations during accretion for Ni, V and Si using P-T-FeO conditions defined in (a) and parameterizations for metal-silicate partitioning from Corgne et al. (2008) for Ni and Si and Wood et al. (2008) for V. Note the large range of final Si core/BSE ratios (yellow path). (c) Expected variations of $\Delta^{30}Si_{BSE\text{-}Chond.}$ showing an important level of uncertainty at the end of accretion, due to large uncertainties in elemental metal-silicate partitioning. Note that the prediction is independent from the type of chondrite chosen as reference.

937

938 Fig. 6: Variations of the $\Delta^{30}Si_{BSE–Chond.}/F_{Core}$ ratio during continuous core formation for
939 several FeO_{BSE} paths (insert, same abscissa) satisfying constraints from moderately
940 siderophile elements. The blue dashed curve is the three-step model proposed by Wood et al.
941 (2008) and considered in Fig. 5. Taking into account the uncertainty on elemental metal-
942 silicate Si partitioning, $\Delta^{30}Si_{BSE–Chond.}/F_{Core}$ lies along a restricted range at the end of accretion
943 (0.88 ± 0.11), regardless of the chosen FeO path.
944

945 Fig. 7: Predicted Si core (wt.%) concentrations as a function of measured $\Delta^{30}Si_{BSE\text{-}Chond.}$. The
946 model (thick curve) is computed using $\Delta^{30}Si_{BSE\text{-}Chond.}/F_{Core} = 0.88$ (see text and Fig. 6). Thin
947 curves show the $\pm$ 0.11 variability of $\Delta^{30}Si_{BSE\text{-}Chond.}/F_{Core}$, which includes the uncertainties on
948 both fO_2 and T variations during the Earth accretion. Experimental constraints (Shahar et al.,
949 2009) and metal-silicate Si isotope partitioning in natural samples (Ziegler et al., 2010) were
950 also taken into account. Any mix of chondrite (whatever their type) shall lead to a $\Delta^{30}Si_{BSE\text{-}}$
951 $_{Chond.}$ that falls on the red section of the curves. The model indicates that the initial $\Delta^{30}Si_{BSE\text{-}}$
952 $_{Chond.}$ should have been 0.12 if one assumes a maximum possible Si core concentration of
953 7wt% after mantle-core differentiation, which is below the minimum value given by O/C-
954 chondrites (0.18). Hence, mantle-core differentiation alone cannot explain the observed
955 different Si isotope composition between chondrites and the bulk silicate Earth if the accreted
956 materials had the composition of chondrites.
957

958 Fig. 8: A) Rayleigh models predicting the variations of $\delta^{30}Si_{Chond.}$ during a vaporization
959 process that may have occurred along with giant interplanetary impact. The equation is
960 defined as $\delta^{30}Si_{Solid\ residue} = \delta^{30}Si_{Chond.} \times (\alpha^{30}_{Si}\text{-}1) \times \ln(f)$, where α is the fractionation factor
961 of Si and f is the fraction of Si remaining in the residual solid. The computation involves a Si
962 isotope fractionation factor during vaporization $\alpha^{29}_{Si} = 0.98985 \pm 0.00044$ (Knight et al.,
963 2009), which has been converted into $\alpha^{30}_{Si} = 0.97893 \pm 0.00088$, assuming the fractionation
964 process is mass dependent. Starting $\delta^{30}Si_{Chond.}$ values were calculated from sample
965 measurements and considered as $\delta^{30}Si_{Bulk\ Earth}$. $\delta^{30}Si_{Chond.}$ values were calculated using E-
966 chondrites (blue), or O/C-chondrites (red). Solid lines represent the corresponding Rayleigh
967 models. The paths delimited by dashed lines takes into considerations both the uncertainties
968 on $\delta^{30}Si_{Chond.}$ averages and α^{30}_{Si}. The intersection between the model and the black solid line
969 ($\delta^{30}Si_{BSE}$ value) gives the fraction Si remaining in the Earth residue at the end of the

vaporization process (*i.e.*, when $\Delta^{30}Si_{BSE\text{-}Chond.} = 0$). These 2 models do not consider Si isotope fractionation from mantle-core differentiation, and therefore are considered as an extreme case. B) The same Rayleigh models assuming that the mantle-core differentiation fractionated Si isotopes prior to vaporization, and the Earth's core incorporated 7wt% Si (thus leading to a 0.12‰ decrease of the $\Delta^{30}Si_{BSE\text{-}Chond.}$ value (Fig. 7) translated on the figure into a 0.12‰ shift on the starting materials). According to these latter models, between 0.4 and 1.1wt% on average of Si loss by vaporization is enough to reconcile a chondritic Earth with isotopic observations while keeping a reasonable amount of Si in the core.

Table Captions:

Table 1: Silicon concentration and isotope data for the Earth, Moon and meteorite samples. Uncertainties are given as ± 2SE, computed as $2SD/\sqrt{(n-1)} \times t$, where t is the Student's correcting factor (Platzner et al., 1997) and where n is the number of replicate analyses of a sample. With the exception of Enstatite chondrites, uncertainties on planetary average values are also given as 2SE, computed using the same relation, where n means the number of individual samples (see text for justification). **Given the E-chondrite dataset only gathers 2 samples, a propagated uncertainty calculation was adopted for these data instead of the 2SE calculation. °Data from Zambardi and Poitrasson (2011). *Sample not included in the bulk-silicate-body average calculation. For averages, N means the number of samples.

Table 2: Si-core concentrations inferred from our model on all available $\Delta^{30}Si_{BSE\text{-}Chond.}$ data from recent literature and this study. All $\Delta^{30}Si_{BSE\text{-}Chond.}$ uncertainties were propagated from the 2SE of both $\delta^{30}Si_{BSE}$ and $\delta^{30}Si_{Chond.}$. All extreme Si-core concentrations include uncertainties from both the model and the $\Delta^{30}Si_{BSE\text{-}Chond.}$ estimates. *Data computed using the $\delta^{30}Si_{BSE\ (Mean)}$ from Savage et al. (2010), see Table 2 in Armytage et al. (2011). **Data computed using an averaged E-chondrites (EH and EL) $\delta^{30}Si_{EC} = -0.67 \pm 0.04$ (2SE, n=13) from Savage and Moynier (2013). ***Data computed from the average of all available analysis of terrestrial and chondrites samples in recent literature, with the exception of Georg et al. (2007) and Chakrabarti and Jacobsen (2010a) data. The $\delta^{30}Si_{BSE}$ also includes all data from Savage et al. (2010).

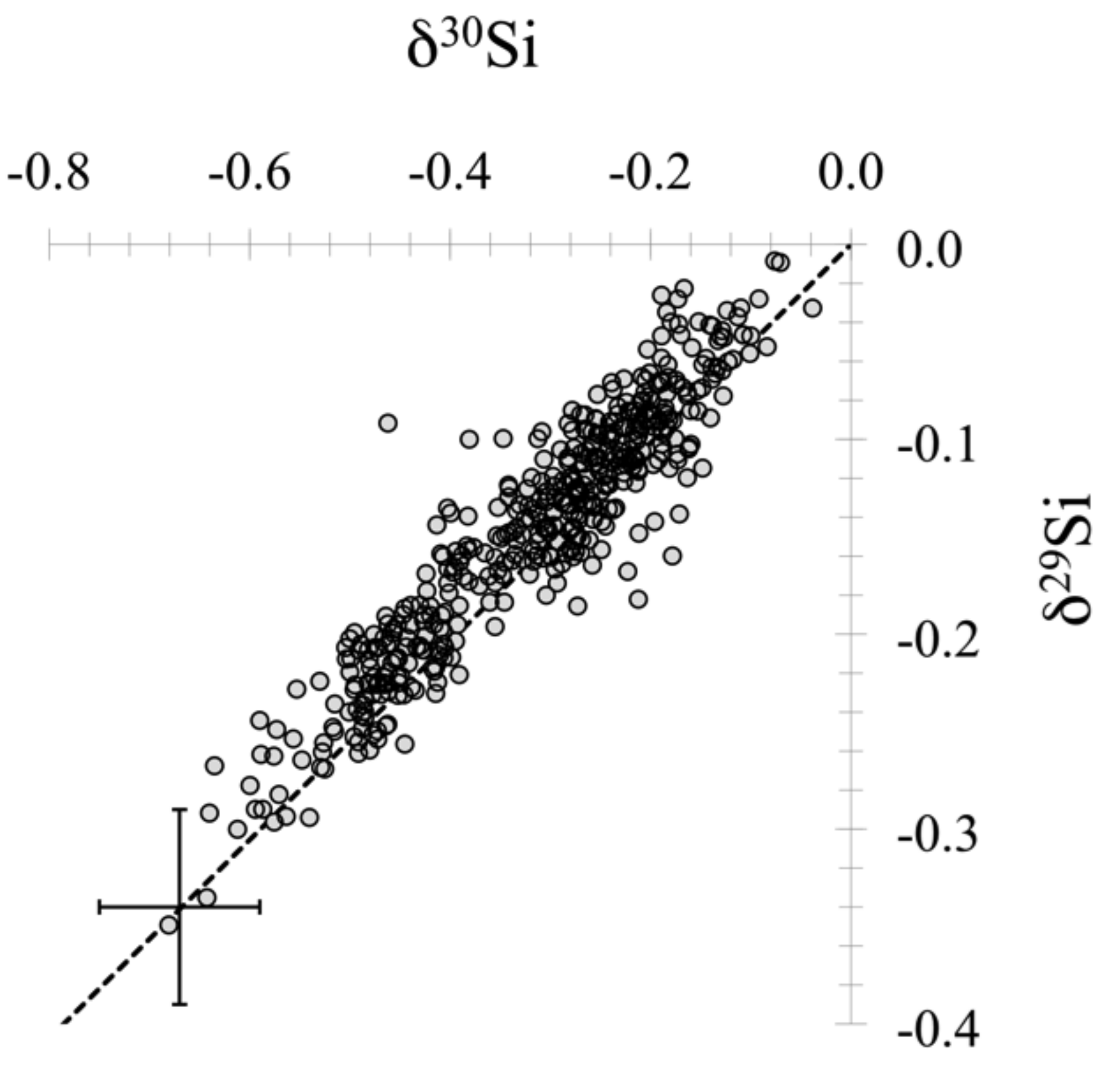
δ30Si
-0.8
-0.6
-0.4
-0.2
0.0
0.0
-0.1
-0.2
-0.3
-0.4
δ29Si

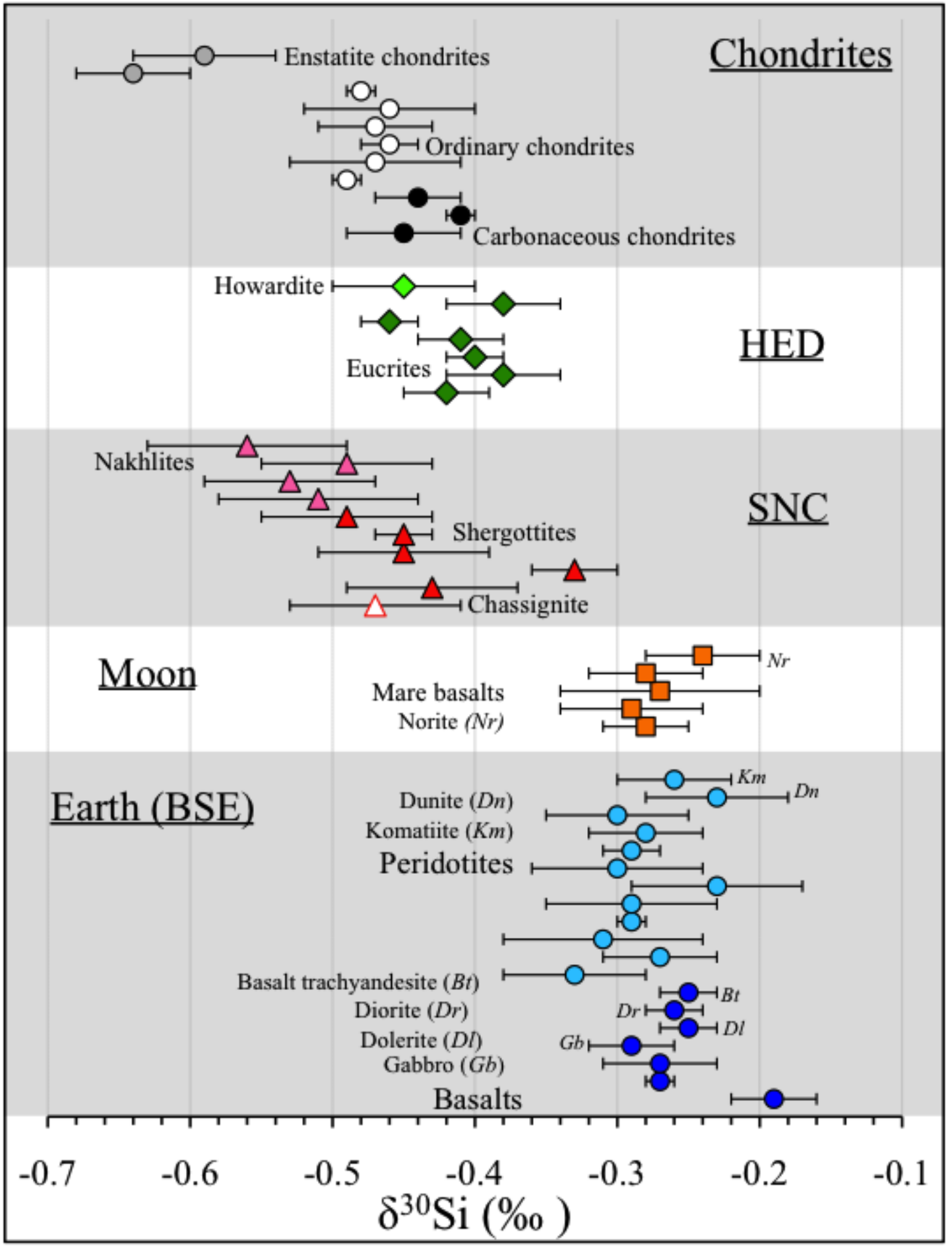
Chondrites
Enstatite chondrites
Ordinary chondrites
Carbonaceous chondrites
HED
Howardite
Eucrites
SNC
Nakhlites
Shergottites
Chassignite
Moon
Mare basalts
Norite (Nr)
Nr
Earth (BSE)
Dunite (Dn)
Komatiite (Km)
Peridotites
Km
Dn
Basalt trachyandesite (Bt)
Diorite (Dr)
Dolerite (Dl)
Gabbro (Gb)
Basalts
Bt
Dr
Dl
Gb
-0.7
-0.6
-0.5
-0.4
-0.3
-0.2
-0.1
δ30Si (‰)

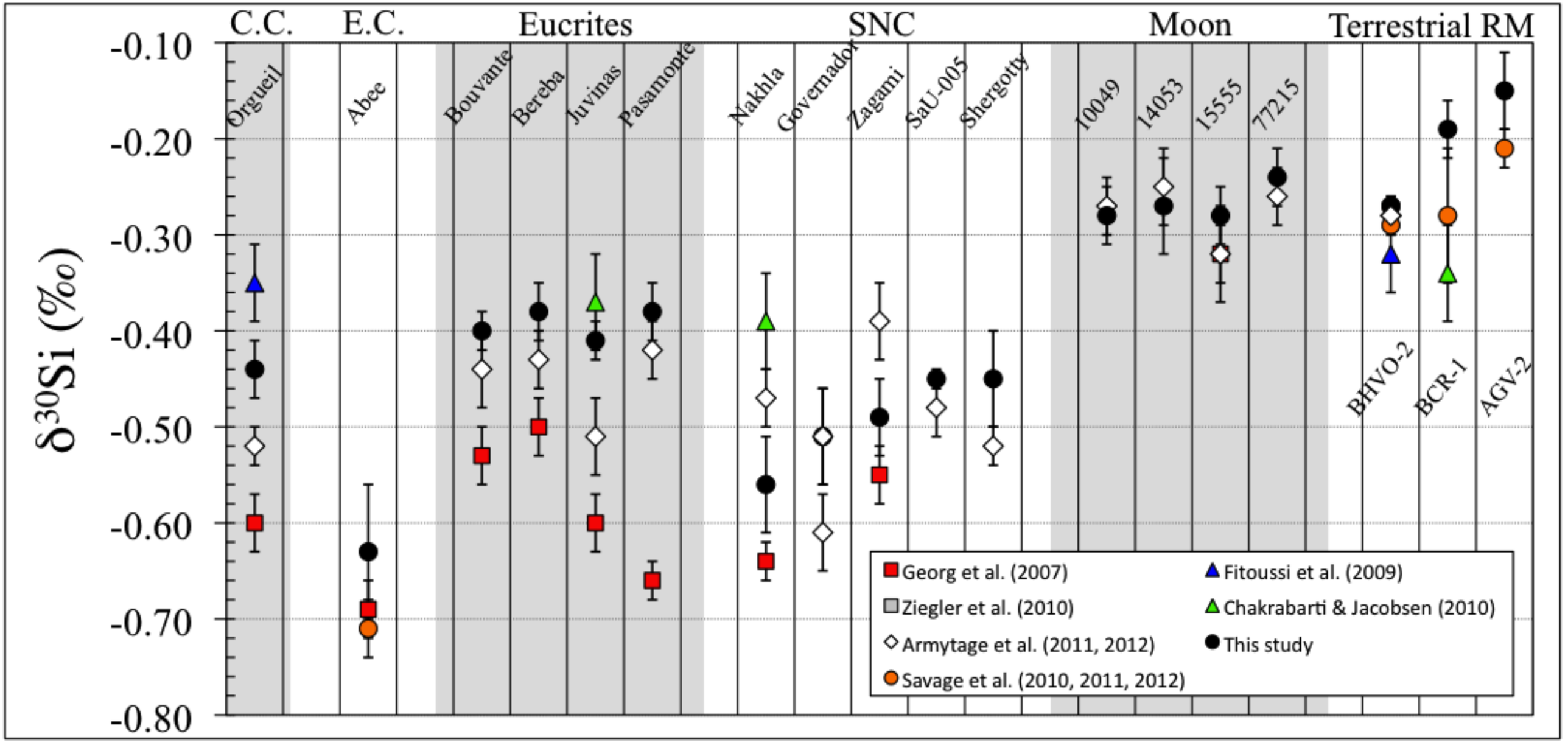
C.C.
E.C.
Eucrites
SNC
Moon
Terrestrial RM
Orgueil
Abee
Bouvante
Bereba
Juvinas
Pasamonte
Nakhla
Governador
Zagami
SaU-005
Shergotty
10049
14053
15555
77215
BHVO-2
BCR-1
AGV-2
δ30Si (‰)
-0.10
-0.20
-0.30
-0.40
-0.50
-0.60
-0.70
-0.80
Georg et al. (2007)
Fitoussi et al. (2009)
Ziegler et al. (2010)
Chakrabarti & Jacobsen (2010)
Armytage et al. (2011, 2012)
This study
Savage et al. (2010, 2011, 2012)

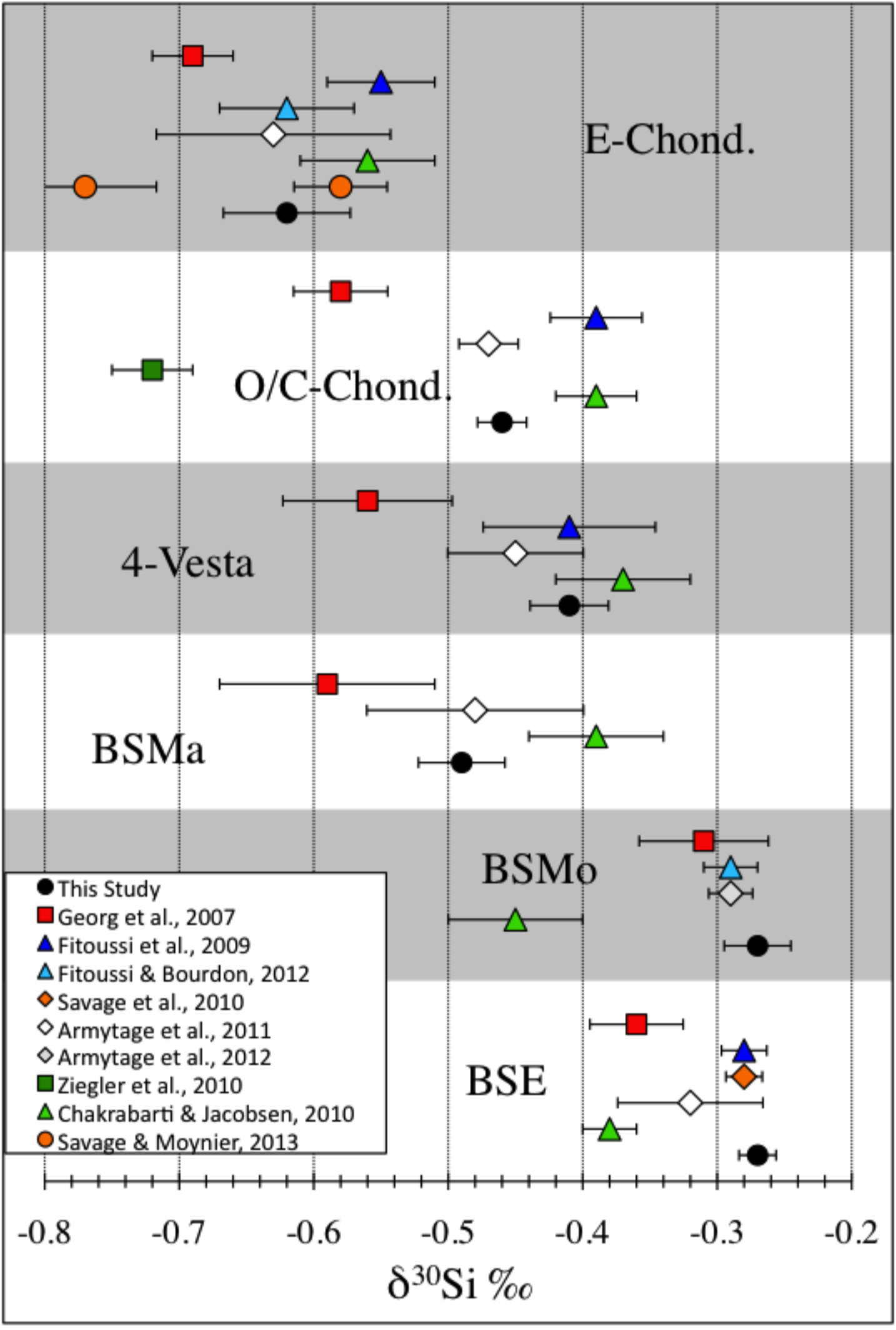
E-Chond.
O/C-Chond.
4-Vesta
BSMa
BSMo
BSE
This Study
Georg et al., 2007
Fitoussi et al., 2009
Fitoussi & Bourdon, 2012
Savage et al., 2010
Armytage et al., 2011
Armytage et al., 2012
Ziegler et al., 2010
Chakrabarti & Jacobsen, 2010
Savage & Moynier, 2013
-0.8
-0.7
-0.6
-0.5
-0.4
-0.3
-0.2
δ30Si ‰

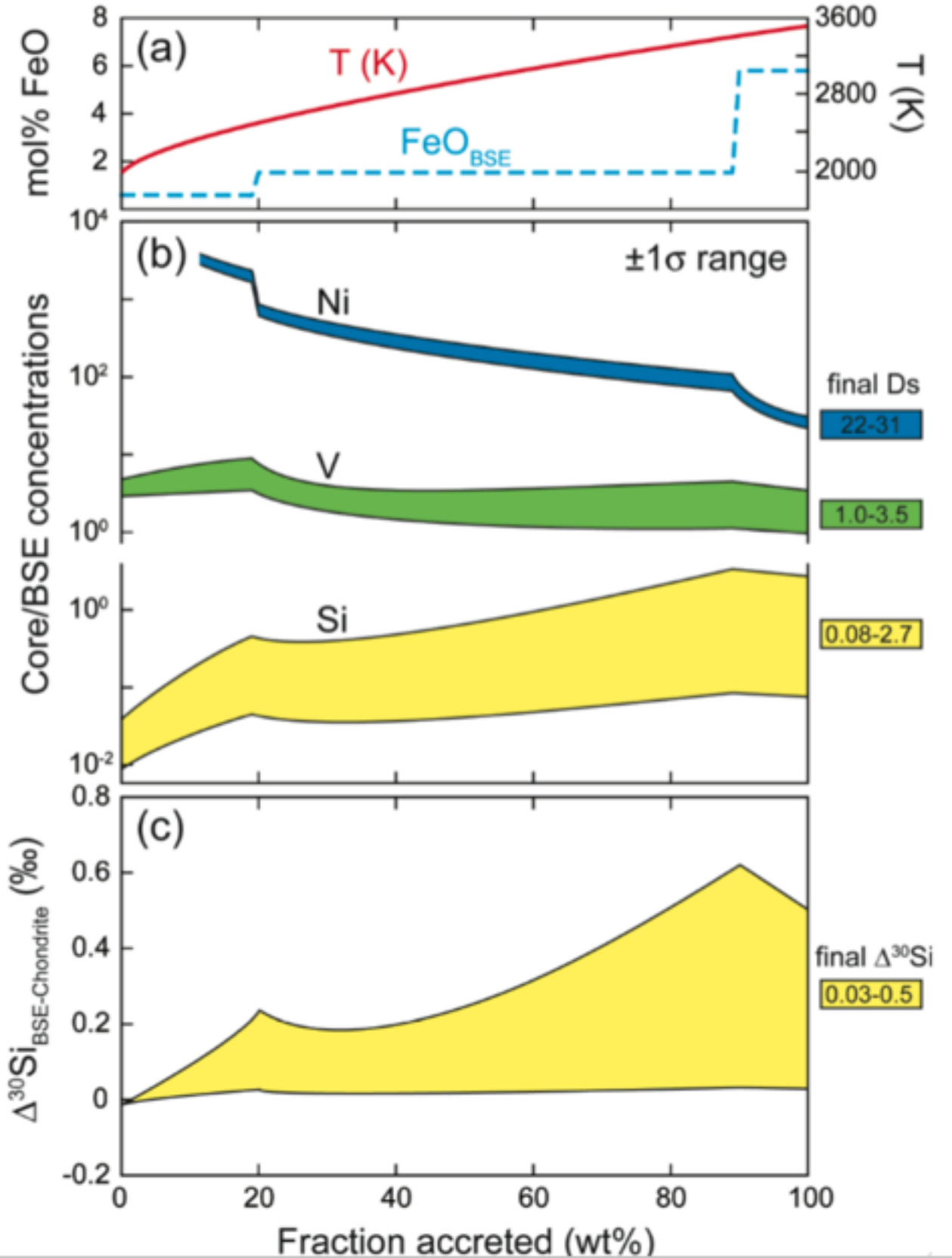
(a)
T (K)
FeO$_{BSE}$
mol% FeO
T (K)
(b)
±1σ range
Ni
V
Core/BSE concentrations
final Ds
22-31
1.0-3.5
Si
0.08-2.7
(c)
$\Delta^{30}Si_{BSE-Chondrite}$ (‰)
final Δ^{30}Si
0.03-0.5
Fraction accreted (wt%)

$\Delta^{30}Si_{BSE-Chondrite} / F_{Si}$

2
1.8
1.6
1.4
1.2
1
0.8
0.6

0
20
40
60
80
100

Fraction accreted %

FeO_{BSE} (mol%)

2.5
2
1.5
1
0.5
0

0
20
40
60
80
100

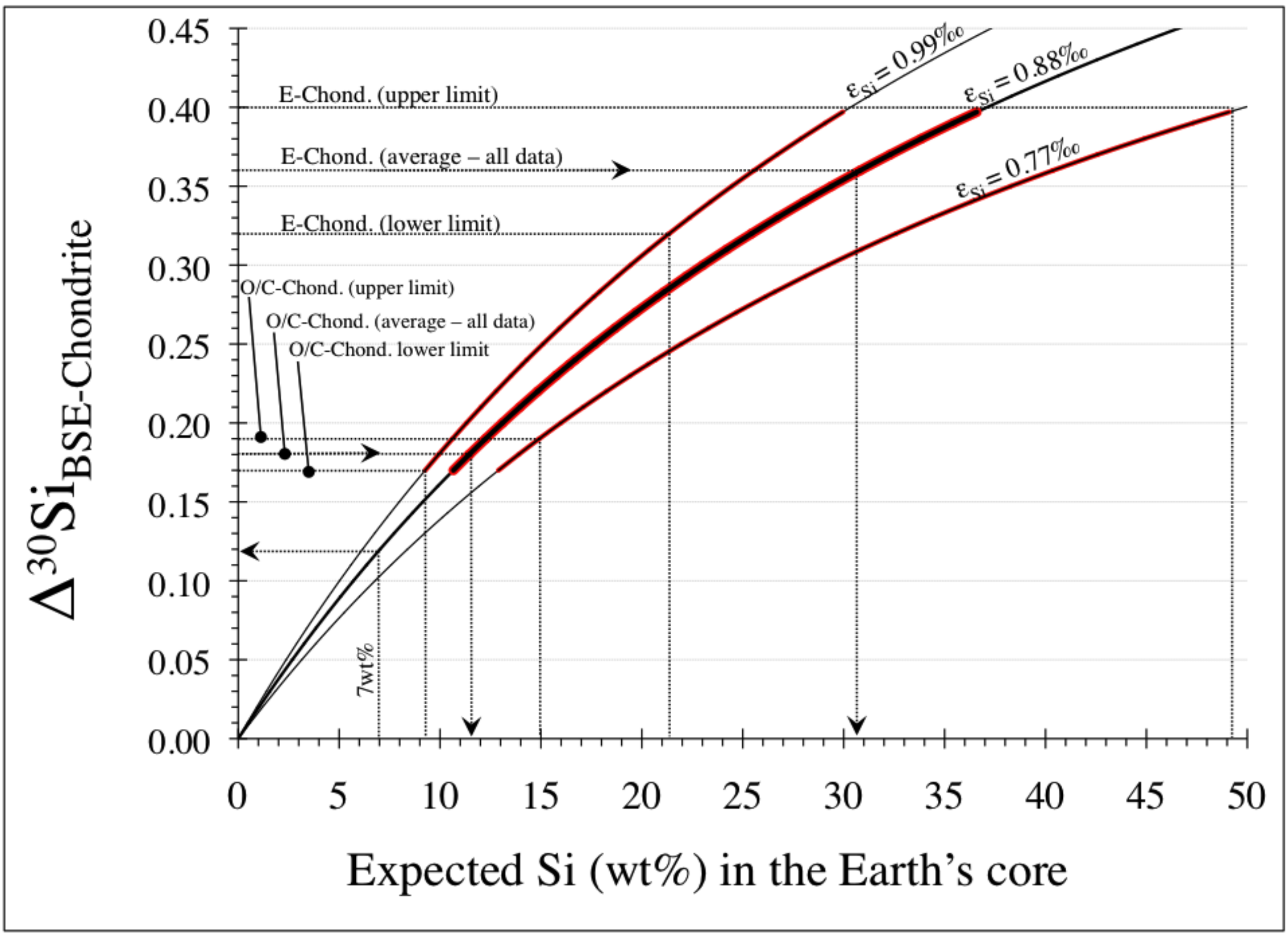
0.45
0.40
0.35
0.30
0.25
0.20
0.15
0.10
0.05
0.00
$\Delta^{30}Si_{BSE-Chondrite}$
E-Chond. (upper limit)
E-Chond. (average – all data)
E-Chond. (lower limit)
O/C-Chond. (upper limit)
O/C-Chond. (average – all data)
O/C-Chond. lower limit
$\varepsilon_{Si} = 0.99‰$
$\varepsilon_{Si} = 0.88‰$
$\varepsilon_{Si} = 0.77‰$
7wt%
0
5
10
15
20
25
30
35
40
45
50
Expected Si (wt%) in the Earth's core

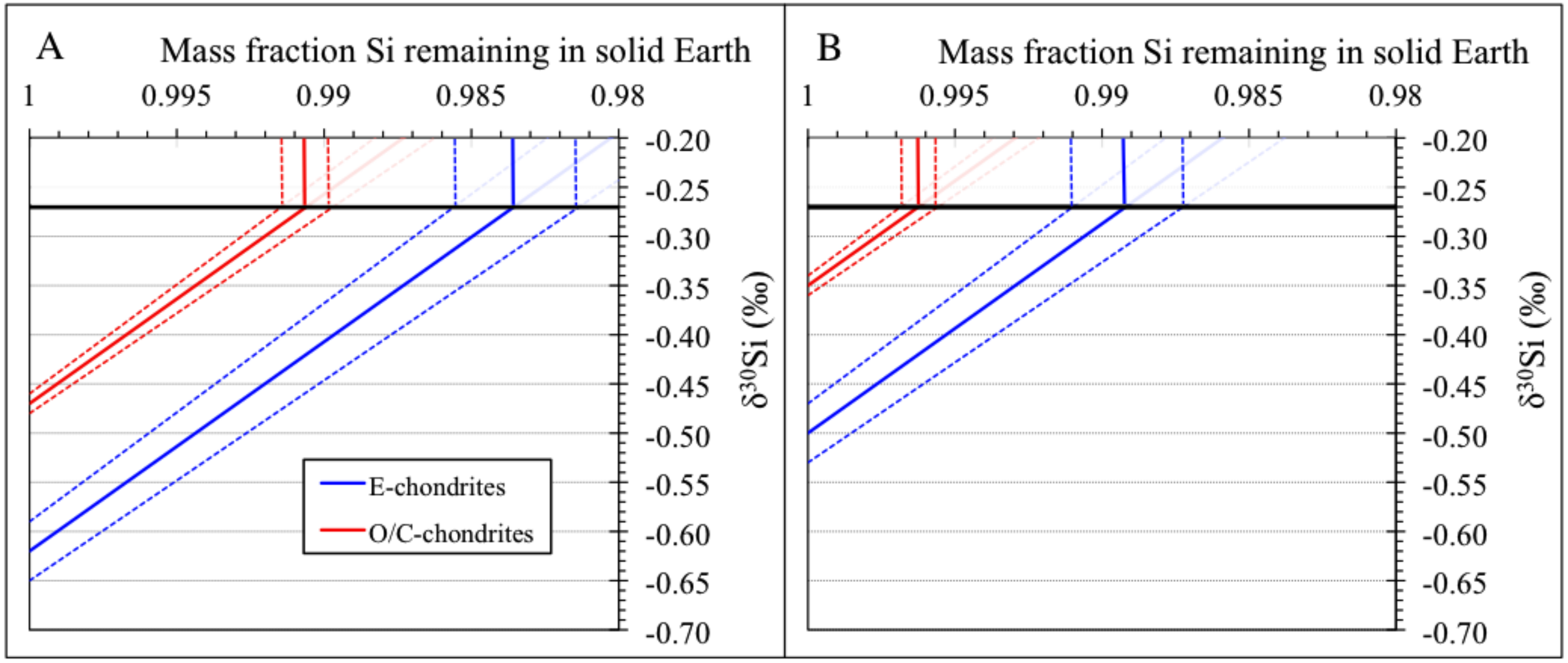
A
Mass fraction Si remaining in solid Earth
1
0.995
0.99
0.985
0.98
-0.20
-0.25
-0.30
-0.35
-0.40
-0.45
-0.50
-0.55
-0.60
-0.65
-0.70
δ30Si (‰)
E-chondrites
O/C-chondrites
B
Mass fraction Si remaining in solid Earth
1
0.995
0.99
0.985
0.98
-0.20
-0.25
-0.30
-0.35
-0.40
-0.45
-0.50
-0.55
-0.60
-0.65
-0.70
δ30Si (‰)

Samples	Nature	Location	SiO_2 (wt%)	$\delta^{30}Si$ (‰)	2SE	$\delta^{29}Si$ (‰)	2SE	n# analyses
Terrestrial mafic rocks (BSE)								
°BCR-2	Basalt	Columbia river, USA	54.0	**-0.19**	0.03	**-0.11**	0.03	6
°BHVO-2	Basalt	Hawaï, USA	49.9	**-0.27**	0.01	**-0.14**	0.01	54
°BIR-1	Basalt	Reikjavik, Iceland	48.0	**-0.27**	0.04	**-0.12**	0.02	6
°PMS	Microgabbro	Pitscurrie, UK	46.9	**-0.29**	0.03	**-0.14**	0.02	6
°OU-2	Dolerite	Belford, UK	51.0	**-0.25**	0.02	**-0.11**	0.02	6
°DR-N	Diorite	Neuntelstein, France	52.9	**-0.26**	0.02	**-0.12**	0.03	6
°ES-9104	Basalt Trachyandesite	Massif d'Esterel, France	52.3	**-0.25**	0.02	**-0.11**	0.02	12
GM92-234	Peridotite	Kerguelen Island	42.2	**-0.33**	0.05	**-0.16**	0.02	3
GR97-38	Peridotite	Kerguelen Island	44.6	**-0.27**	0.04	**-0.12**	0.02	3
GR97-52	Peridotite	Kerguelen Island	44.6	**-0.31**	0.07	**-0.14**	0.04	3
JGM-92-1c	Peridotite	Kerguelen Island	42.4	**-0.29**	0.01	**-0.14**	0.02	6
°JP-1	Peridotite	Horoman, Japan	42.4	**-0.29**	0.06	**-0.13**	0.03	6
°KNO3	Peridotite	Cameroon	45.0	**-0.23**	0.06	**-0.11**	0.04	6
MG91-3	Peridotite	Kerguelen Island	39.6	**-0.30**	0.06	**-0.16**	0.04	3
NK-01	Peridotite	Cameroon	43.5	**-0.29**	0.02	**-0.14**	0.01	3
PREM89-1	Peridotite	South Africa	40.9	**-0.28**	0.04	**-0.14**	0.04	3
PREM90-24	Peridotite	South Africa	40.9	**-0.30**	0.05	**-0.15**	0.02	3
°DTS-2b	Dunite	Bellingham, USA	39.4	**-0.23**	0.05	**-0.10**	0.04	6
°WITS-1	Komatiite	Barberton, South Africa	43.3	**-0.26**	0.04	**-0.11**	0.02	9
Average BSE				**-0.27**	**0.01**	**-0.13**	**0.01**	N=19
Lunar samples								
10049	High Ti mare basalt	1969, Mare Tranquillitatis	42.0	**-0.28**	0.03	**-0.13**	0.02	7
12054	Ilmenite basalt	1969, Oceanus Procellarum	42.2	**-0.29**	0.05	**-0.13**	0.01	9
14053	Low Ti mare basalt	1971, Fra Mauro	46.3	**-0.27**	0.07	**-0.10**	0.02	6
15555	Olv. normative mare basalt	1971, Hadley Apennines	44.6	**-0.28**	0.04	**-0.13**	0.02	8
77215	Cataclastic norite	1972, Taurus Littrow	51.2	**-0.24**	0.04	**-0.10**	0.03	6
Average BSMo				**-0.27**	**0.02**	**-0.12**	**0.02**	N=5
Carbonaceous chondrites								
NWA-1757	CO3	Find 2001, Morocco	34.1	**-0.45**	0.04	**-0.21**	0.03	6
NWA-4425	CK3	Find 2006, Algeria	33.4	**-0.41**	0.01	**-0.20**	0.04	3
Orgueil	CI1	Fall 1864, France	20.1	**-0.44**	0.03	**-0.23**	0.02	12
Ordinary chondrites								
Acfer-380	H5	Find 2002, Algeria	36.2	**-0.49**	0.01	**-0.25**	0.02	3
NWA-2258	L5	Find 2001, Algeria	35.6	**-0.47**	0.06	**-0.23**	0.03	6
NWA-4278	L6	Find 2005, Morocco	40.3	**-0.46**	0.02	**-0.21**	0.02	6
NWA-4260	L6	Find 2003, Algeria	34.9	**-0.47**	0.04	**-0.20**	0.02	12
Mocs	L6	Fall 1882, Romania	38.4	**-0.46**	0.06	**-0.21**	0.03	6
Tanezrouft-065	L4	Find 2002, Algeria	39.6	**-0.48**	0.01	**-0.24**	0.05	3
Average O/C-Chond.				**-0.46**	**0.02**	**-0.22**	**0.02**	N=9
Enstatite chondrites								
Abee	EH	Fall 1952, Canada	41.1	**-0.64**	0.04	**-0.33**	0.07	3
St sauveur	EH	Fall 1914, France	35.4	**-0.59**	0.05	**-0.30**	0.01	3
Average E-Chond.				**-0.62**	***0.04*****	**-0.32**	***0.03*****	N=2
Mars (SNC)								
Chassigny	Chassignite, dunite	Fall 1815, France	36.0	**-0.47**	0.06	**-0.21**	0.02	7
DaG-476	Shergottite, Ol-phyric basalt	Find 1999, Lybia	45.4	**-0.43**	0.03	**-0.20**	0.03	5
Los Angeles*	Shergottite, Px-phyric basalt	Find 1980, CA USA	48.6	**-0.33**	0.06	**-0.16**	0.02	5
SaU-005	Shergottite, Ol-phyric basalt	Find, Oman	46.3	**-0.45**	0.02	**-0.21**	0.02	5

Shergotty	Shergottite, Px-phyric basalt	Fall 1865, India	49.5	**-0.45**	0.06	**-0.21**	0.05	5
Zagami	Basalt Shergottite	Fall 1962, Nigeria	49.7	**-0.49**	0.05	**-0.21**	0.06	7
Governador	Nakhlite, cpxnite	Find 1958, Brasil	48.0	**-0.51**	0.07	**-0.23**	0.04	5
Lafayette	Nakhlite, cpxnite	Find 1931, USA	46.5	**-0.53**	0.06	**-0.25**	0.03	8
MIL-03 346	Nakhlite, cpxnite	Find 2003, Antarctica	49.1	**-0.49**	0.06	**-0.21**	0.02	5
Nakhla	Nakhlite, cpxnite	Fall 1911, Egypt	48.0	**-0.56**	0.07	**-0.25**	0.02	5
Average BSMa				**-0.49**	**0.03**	**-0.22**	**0.01**	N=9
4-Vesta (HED)								
ALHA-78132	Eucrite	Find 1978, Antarctica	49.9	**-0.42**	0.03	**-0.20**	0.04	6
Bereba	Eucrite	Fall 1924, Burkina Faso	52.7	**-0.38**	0.04	**-0.15**	0.03	6
Bouvante	Eucrite	Find 1978, France	50.1	**-0.40**	0.02	**-0.19**	0.03	6
Juvinas	Eucrite	Fall 1821, France	50.6	**-0.41**	0.03	**-0.18**	0.02	7
NWA-1777	Eucrite	Find 2002, Algeria	49.9	**-0.46**	0.02	**-0.21**	0.02	6
Pasamonte	Eucrite	Fall 1933, NM USA	49.3	**-0.38**	0.04	**-0.17**	0.03	6
Le Teilleul	Howardite	Fall 1845, France	49.9	**-0.45**	0.05	**-0.20**	0.02	6
Average 4-Vesta				**-0.41**	**0.03**	**-0.19**	**0.01**	N=7

Table 2

	$\Delta^{30}Si_{BSE\text{-}O/CC}$	Si-core conc. (wt.%)	$\Delta^{30}Si_{BSE\text{-}EC}$	Si-core conc. (wt.%)
Georg et al. (2007)	0.20 ± 0.05	13^{+9}_{-5}	0.31 ± 0.04	24^{+14}_{-7}
Fitoussi et al. (2009)	0.11 ± 0.04	6^{+5}_{-3}	0.27 ± 0.05	20^{+13}_{-7}
Chakrabarti and Jacobsen (2010a)	0.02 ± 0.04	1^{+3}_{-1}	0.18 ± 0.05	12^{+8}_{-5}
Armytage et al. (2011)	0.15 ± 0.05	9^{+7}_{-5}	0.31 ± 0.09	24^{+26}_{-11}
	0.19 ± 0.01*	12^{+4}_{-2}	0.35 ± 0.08*	29^{+29}_{-12}
Fitoussi and Bourdon (2012)	-	-	0.34 ± 0.05	28^{+17}_{-9}
Savage and Moynier (2013)	-	-	0.39 ± 0.04**	35^{+24}_{-11}
This study	0.19 ± 0.01	12^{+4}_{-2}	0.35 ± 0.05	29^{+21}_{-9}
All data* **	0.18 ± 0.01	12^{+3}_{-3}	0.36 ± 0.04	31^{+19}_{-10}